Design and Implementation of a Terahertz Antenna for a Nanocontact Based Photomixer

Entwurf und Herstellung einer Terahertzantenne für einen Nanokontaktbasierten Photomixer

Author:	**Verónica Laín Rubio**
Degree Programme:	**Information and Communication Engineering**
Examiner:	**Prof. Dr. Thomas Kusserow**
Department:	**Institute for Microwaves and Photonics**
Supervisor:	**Dr. Ing. Shihab Al-Daffaie**
Start Date:	**12.11.2018**
Date Of Submission:	**10.05.2019**
Examination Date:	**24.05.2019**
Masterthesis	**(2283-M)**

TECHNISCHE UNIVERSITÄT DARMSTADT

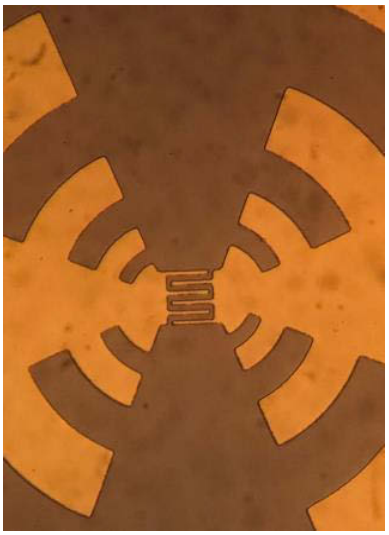

Affidavit/Eidesstattliche Versicherung

Erklärung zur Abschlussarbeit gemäß §22 Abs. 7 und §23 Abs. 7 APB TU Darmstadt
Hiermit versichere ich, Verónica Laín Rubio, die vorliegende Master-Thesis / Bachelor-Thesis gemäß §22 Abs. 7 APB der TU Darmstadt ohne Hilfe Dritter und nur mit den angegebenen Quellen und Hilfsmitteln angefertigt zu haben. Alle Stellen, die Quellen entnommen wurden, sind als solche kenntlich gemacht worden. Diese Arbeit hat in gleicher oder ähnlicher Form noch keiner Prüfungsbehörde vorgelegen.
Mir ist bekannt, dass im Falle eines Plagiats (§38 Abs.2 APB) ein Täuschungsversuch vorliegt, der dazu führt, dass die Arbeit mit 5,0 bewertet und damit ein Prüfungsversuch verbraucht wird. Abschlussarbeiten dürfen nur einmal wiederholt werden.
Bei der abgegebenen Thesis stimmen die schriftliche und die zur Archivierung eingereichte elektronische Fassung gemäß §23 Abs. 7 APB überein.

Place, Date	Author

Zusammenfassung/Abstract

In dieser Masterarbeit wird ein Design einer neuen integrierten Terahertz (THz) Antenne für einen nanokontaktbasierten Photomischer (Nanophotomischer) vorgestellt. Gängige Nanophotomischers in Niedertemperatur (LTG) -GaAs sind breitbandige und kompakte THz-Quellen dessen Leistung mit der nutzung von nanokontakte, durch die Überwindung ihre Ausfallmechanismen und Verbesserung ihres Photostroms verbessert werden können. Daher können weniger optiche Laserleistung als Eingangsbeatsquelle verwendet werden, die auf kompakte, integrierbare, kostengünstige und einfach herzustellende THz-Quellen umsteigen und auf die tatsächlichen sperrigen und teuren THz-Systeme verzichten. Photomischer weisen jedoch keine Richtwirkung auf, ein Problem, das üblicherweise durch Anbringen einer sperrigen und für Fehlausrichtungen sehr empfindlichen Siliziumlinse an dem Substrat gelöst wird. Daher besteht das Hauptziel dieser Arbeit darin, diese sperrige Siliziumlinse zu ersetzen, um die Integration und Portabilität von THz-Geräten und -Systemen zu ermöglichen. Zu diesem Zweck wurden verschiedene Beugungslinsen in Betracht gezogen: Fresnel-Zonenplatten (FZP), gerillte Linsen und Photonensiebe (PS). In einigen Werken wurden bereits FZPs verwendet [1], hier wurde jedoch ein anderer Ansatz zur Integration und Größenreduzierung gewählt. Im Verlauf der Dissertation werden verschiedene Designs vorgestellt, die zum endgültigen Gerät führen, dass für die Implementierung ausgewählt wurde. Dieses auf FZP basierende Design hat in den Simulationen einen hohen Richtwirkungsgrad bei einer Frequenz von 1067 GHz, einen breiten Arbeitsfrequenzbereich und eine Robustheit gegen Fehlausrichtungen gezeigt. Darüber hinaus sind für diese integrierte Vorrichtung nur zwei einfache Verarbeitungsschritte der Herstellungstechnologie (normale optische Lithographie) erforderlich, wodurch auch eine einfache und skalierbare Implementierung erreicht wird.

A new design of an integrated Terahertz (THz) lens-antenna for a nanocontact based photomixer (nanophotomixer) is presented in this Master Thesis. THz nanophotomixers in Low Temperature (LTG)-GaAs are broadband and compact THz sources in which the use of nanocontacts has improved their performance, overcoming their failure mechanisms and enhancing their photocurrent. Thus, less optical laser power can be used as input beat source, moving towards compact, integrable, low-cost and easy to fabricate THz sources, abandoning the actual bulky and expensive THz systems. However, the issues of directivity and coupling of the THz power are commonly solved by attaching a bulky and very sensitive to misalignments silicon lens to the photomixer substrate. Therefore, the main goal of this work is to substitute this bulky silicon lens, allowing integration and portability of THz nanodevices and systems. In order to do so, different diffraction lenses have been considered: Fresnel Zone Plates (FZP), grooved lenses and Photon Sieves (PS). FZPs have already been used in some works [1], but a different approach has been taken here towards simpler integration and size reduction. Throughout the dissertation, different designs are presented, concluding to the final device that has been chosen to be implemented. This FZP-based design has shown in the simulations a high directivity value at a frequency of 1067 GHz, a broad working frequency range and a robustness against misalignments. Moreover, only two simple fabrication technology processing steps (normal optical lithography) are needed for this integrated device, achieving also an easy and scalable implementation.

Contents

1 Introduction

The range of Terahertz (THz) frequencies is located between 100 GHz and 10 THz, directly between the microwave and infrared (IR) frequency ranges. This position in the spectrum gives THz waves some special properties like low photonic energy, high water absorption or large bandwidth, that appear to be really interesting for determined applications. Therefore, THz applications can be found in different fields such as imaging technology, biomedical engineering, security, spectroscopy or material characterization. Also, they could be used in the future as short-distance wireless communications taking into account some advantages they present compared with microwaves.

Actual THz systems are formed by some type of THz emitter and receiver and a set of mirrors and reflectors to conduct the wave, which make them bulky, expensive and not portable. Regarding the emitter, in which this work will be centred, different types can be found, depending on the kind of wave generation it is used: electrical up conversion, direct generation or optical-down conversion. Conventional photomixers are included in this last type because they use optically illuminated electrodes on a high-speed photo-conductive material, such as low-temperature-grown-GaAs (LTG-GaAs), for THz generation. The generated carriers between the electrodes are transferred and coupled to a suitable antenna for THz radiation.

In order to overcome the failure mechanisms of the conventional photomixer, nanocontacts have been used and reported in [2]. Moreover, they produce a large reduction of the capacitance and increase the photocurrent as compared to conventional photomixers. Thus, since the photocurrent is enhanced, less power from the source is needed and, therefore, less optical laser power can be used as input beat source, evolving towards compacter, on chip systems.

However, the generated THz signal requires an additional coupling media in order to have certain directivity. Thus, a bulky silicon lens is used normally in such THz devices in order to easily achieve some characteristics of interest, like directivity or modifications in phase or amplitude. The bulkiness of these kind of lenses makes it impossible to have more compact sources, nor portable applications. Furthermore, since these lenses are external, i.e. not integrated with the photomixer, they are difficult to align with it and big changes in the beam happen with any small misalignment between the lens and the source.

The aim of this work is to find a suitable alternative to the silicon lens, achieving the same or similar directivity characteristics of it, to create broadband, powerful and compact continuous wave (CW) THz sources for actual and future applications. In order to achieve this compactness in the antenna (either receiving or emitting positions), different possible solutions have been studied: Fresnel Zone Plates (FZP), grooved lenses and Photon Sieves (PS). These two diffractive lenses are commonly used in the X-ray range in applications such as microscopy and spectroscopy in physical and life sciences, and they will be described in more detail along the following chapters.

Devices with integrated FZP at the frequencies of THz have already been explored, like in [1], where different substrates were placed between the source and the FZP. However, the structures are still presented as big, due to the necessary thickness of the substrates. In this work a different approach will be taken, trying to avoid the extra thickness and working directly on the LTG-GaAs with different options and designs.

Regarding the structure of this dissertation, in the second chapter, the working process of a typical and a nanocontacts based photomixer and the components that integrate it, will be shown. In the third chapter the considered planar lenses for this work will be explained in detail, including the design equations. Chapters four and five will include a short explanation about the so called moth-aye structure and the Finite Difference Time Domain (FDTD) solving method, respectively. Starting with the designs, chapter six will describe the devices that include a mounted lens, whereas chapter seven will include the devices, where the lens is integrated directly in the substrate. Both, six and seven, will show the corresponding simulations and results achieved. A brief explanation is done in chapter eight regarding the implementation steps that have

to be followed in order to implement the final chosen device elected among the others to be fabricated, as well as the results obtained in this implementation. Finally, conclusions and future work will be included in the last chapter. Furthermore, some appendixes with the python code used for the simulations and the technical drawings for the implemented mask will be found.

2 Nanocontact Based Photomixer

The frequencies between 100GHz and 10THz belong to the range of Terahertz (THz) and they present some special characteristics, like low photonic energy, high water absorption or a large bandwidth, due to their position in the spectrum, between the microwave and infrared frequencies. It is because of that, that THz are suitable for applications in security, imaging, spectroscopy or material characterisation, among others.
THz systems, however, appear to be still bulky and expensive compared with other well-known technologies, not allowing to have portable systems, which would be revolutionary for many applications. Therefore, despite all the possibilities they offer, THz have not yet developed all their potential. One example of these systems can be seen in Fig. 2.1, where two lasers are used to generate the THz wave, together with a photomixer based emitter (and detector) and some mirrors that conduct the wave towards the detector.
Photomixer based emitters belong to the category of optical down conversion THz sources listed in Chapter 1 and can work as an emitter or detector. They are commonly formed by a photomixer integrated in some type of antenna (log-periodic, dipole...) and attached to a bulky silicon lens (Si-lens), which is used in order to improve some characteristics of the generated wave, like directivity or light coupling.
Improvements towards the reduction in size of the source have already been studied by using quantum-cascade lasers or nanowires. However, there is still a part of the photomixer that is making the device bulky and, thus, has to be replaced in order to achieve complete integration: the silicon lens.
This work, therefore, will be centred on the emitter and detector, which structure will be analyzed in detail along this chapter, trying to reduce their sizes, contributing to the general size reduction of the system.

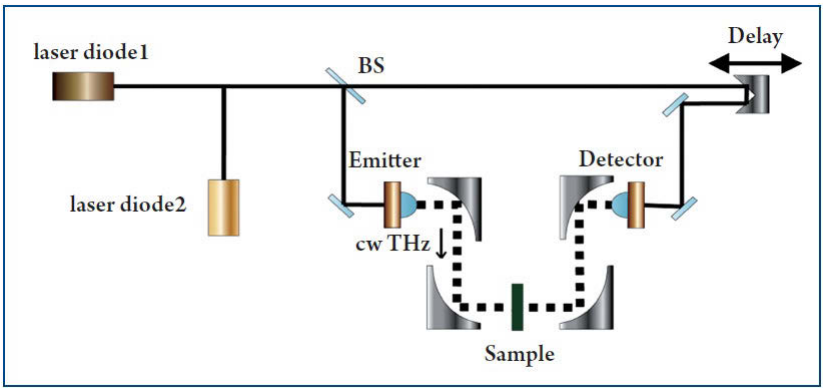

Figure 2.1: An example of a THz system [3]

2.1 Photomixer

Photomixing or optical heterodyne conversion is a technique employed to generate continuous-wave THz radiation by using optically illuminated electrodes on a high-speed photo-conductive material, such as low-temperature-grown (LTG) GaAs. Photomixers are broadband, compact, solid-state sources that commonly use a pair of single-frequency tunable lasers for THz difference frequency generation by photoconductive mixing in LTG-GaAs [4].
For photomixing, the photoconductance is modulated by the optical beating of two laser sources, which difference in frequency must be in the THz range and will define the output frequency. Regarding the output

THz power, it will depend on the incident optical power that provides DC bias between the photoconductor electrodes. Once the semiconductor is biased an electric field $\overrightarrow{E}$ is created to make the carriers drift. For instance, if the photomixer would have interdigitated electrode fingers, as the one presented in Fig. 2.4, the applied electric field would accelerate the photogenerated carriers and the photomixer would collect the mixed signal [5].

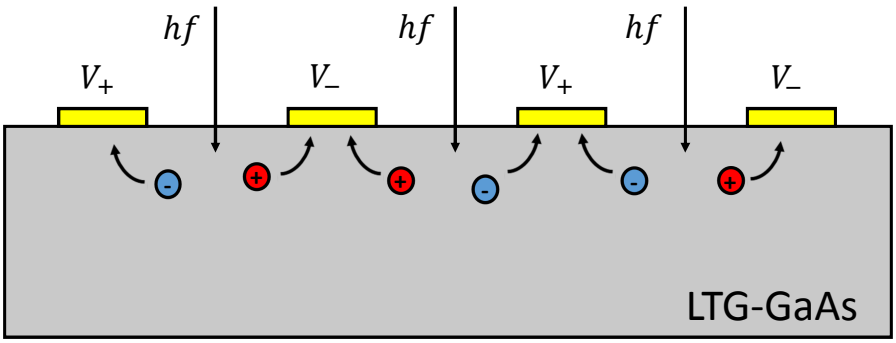

Figure 2.2: Transversal cut of an interdigitated conventional photomixer

In order to overcome the failures of the conventional photomixers, nanocontacts can be used. One example of nanocontact would be the nanowires, which are a 1-D nanomaterial, i.e. the material group that are equivalent in all nanoscale dimensions but in one direction. Moreover, their use reduces the capacitance and increases the photocurrent of the conventional photomixer, as it was shown in [4]. Therefore, less power is needed to generate a high enough photocurrent in the photomixer. Due to this, less powerful and smaller in size lasers can be used, reducing part of the device's size.
The generated carriers between the electrodes are transferred and coupled to a suitable antenna for THz radiation that will be explained in more detail in the following section.

2.2 Antenna

In order to radiate the generated THz wave, the photomixer is integrated in a suitable antenna, which will radiate the charges drifted through the photomixer. Thus, the THz wave will be characterized by the features of the chosen antenna.
Since the desired device required a radiation pattern as broadband as possible, frequency independent antennas have been considered. The shapes of these antennas ideally require infinite structures and their currents should decrease with distance from the feeding points of the antenna. However, they can be cut off at a certain point when the currents become negligible. The resulting antenna will have a lower cut-off frequency in comparison with frequency-dependent antennas and above it, it will have practically identical radiation characteristics than the infinite ideal model. The lowest f_{min} cut-off frequency will depend on the furthest point of the structure, i.e. the point where the current becomes negligible and the highest cut-off frequency f_{max} will be limited by the smallest dimension of the feed transmission line [6].
Log-periodic antennas are close to this type of antenna, but they are not exactly included due to the fact that not all the dimensions can be angle-dependent. However, their characteristics are practically the same and present also a really wide bandwidth. Three types are going to be described along this section: bow-tie antennas, log-periodic tooth antennas and log-periodic spiral antennas. The shape of all these types is shown in (Fig.2.3).

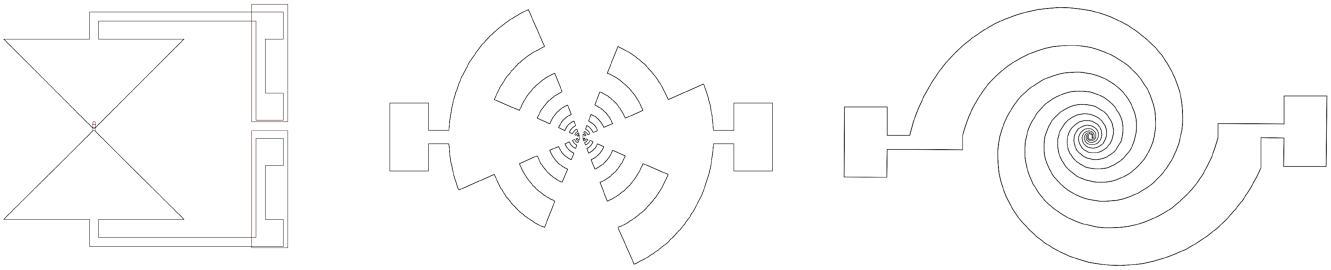

(a) bow-tie antenna. (b) log-periodic tooth antenna. (c) log-periodic spiral antenna.

Figure 2.3: Different types of planar broadband antennas

All these three types of antenna, as explained above, are almost frequency independent since almost all their geometries are specified by angles and, therefore, the working frequency range will be wider than with lambda-dependent antennas, like dipoles. It must be noted that a change in size does not change the performance of the antenna as long as the electrical dimensions remain unchanged, which makes them also suitable for the THz range.
The bow-tie antenna (Fig.2.3a), which has a similar radiation pattern to a dipole antenna, has its first resonance at $f < f_{\frac{\lambda}{2}}$ because, as it was explained above, the antenna is finite, causing an abrupt termination of all currents at its ends, reducing the bandwidth by increasing the lowest usable frequency.
The limitation in bandwidth of the bow-tie antenna can be solved by adding periodically positioned teeth sorting out the current distribution along the antenna by transforming the open end of the tooth into a short when their length corresponds to $\frac{\lambda}{4}$, getting the log-periodic tooth antenna (Fig.2.3b). The bandwidth of this antenna is more than double the bandwidth of the bow-tie, being defined by the longest arm (f_{min}) and the smallest arm (f_{max}).
Regarding the log-periodic spiral antenna (Fig.2.3c), radiation occurs when the currents on the spiral's arms are in phase, getting also a large bandwidth, which lowest cut-off frequency f_{min} will depend on the length of the arms of the spiral.
Due to the bandwidth characteristics exposed, only the log-periodic tooth antenna and the log-periodic spiral antenna will be used in the implementation of the final integrated device.
As mentioned at the beggining of the section, the photomixer is integrated in the antenna. This can be seen in the the following figure (2.4), where an interdigitated photomixer is integrated in a log-periodic spiral antenna.

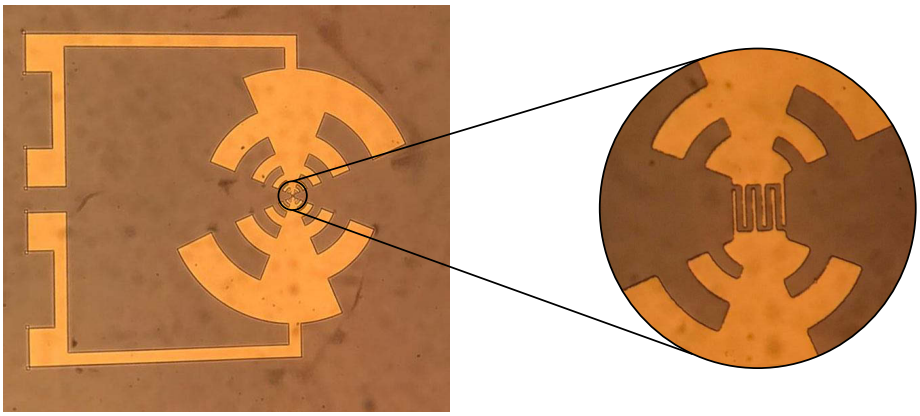

Figure 2.4: Interdigitated photomixer integrated in a log-periodic tooth antenna

In terms of directivity, frequency-independent antennas present a higher value than a traditional dipole,

although it is still not enough for a nanophotomixer based THz source and a lens has to be used, which will be presented in the following section.

2.3 Silicon Lens

As it was mentioned at the beginning of this chapter, a silicon lens is attached to the photomixer in order to improve the performance of the antenna: achieving higher directivity, light coupling and having the possibility to make changes in phase and amplitude.
A lens is preferred in this case to a mirror antenna due to the fact that it is more tolerant to surface errors [7]. Furthermore, silicon is used because of its refractive index ($n \cong 3.43$) [8], which allows to couple the THz wave between the LTG-GaAs substrate and the air. Since the substrate has a similar refractive index ($n \cong 3.59$) [8], which translates into a really high permittivity $\varepsilon_r \cong 12.97$, very few propagation is achieved without a coupling media. Thus, a really easy solution is to mount a silicon lens on the substrate that should have a shape as elliptical as possible, in order to avoid possible substrate modes and to radiate as much power as possible. The elliptical shape of the lens reduces the angle of incidence of the incident wave in comparison with the flat surface of the substrate on its own. Moreover, it redirects the radiated rays towards the boresight direction achieving more directivity and transmission efficiency [9]. In Fig. 2.5 it is shown the difference in performance between a GaAs substrate with and without this silicon lens at a frequency of 1THz, where the devices have been highlighted with a dashed line.

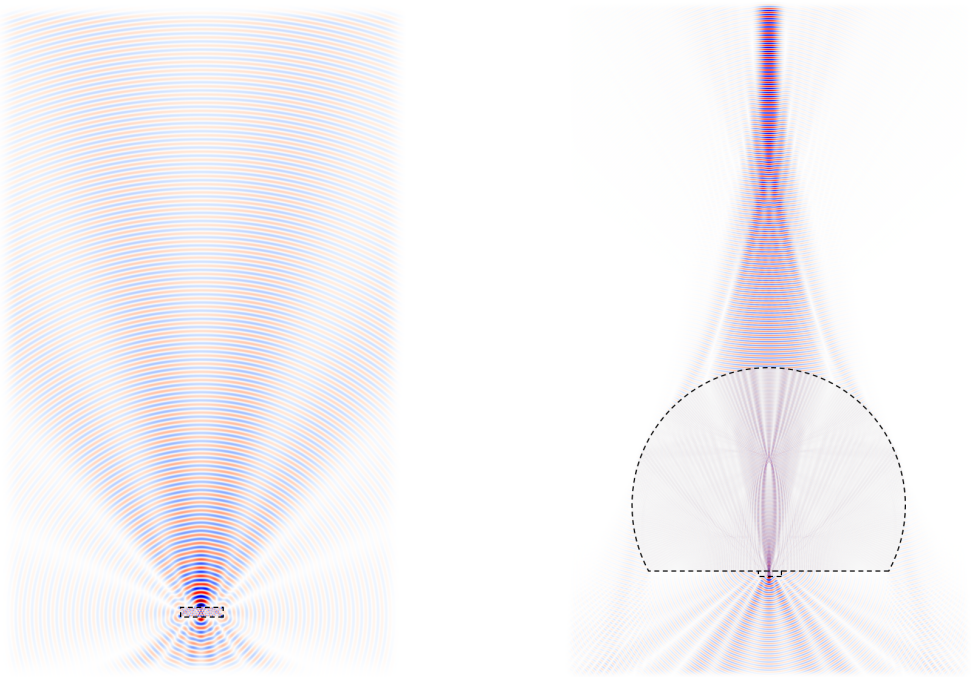

(a) LTG-GaAs

(b) LTG-GaAs with a hyper-hemispherical Si-lens (radius=15mm).

Figure 2.5: Performance of LTG-GaAs without and with silicon lens for f=1THz

Although the silicon lens allows wave propagation and improves the performance of the output wave of the photomixer, it has some major disadvantages. First of all, it makes the whole device really bulky, taking into account that the size of the photomixer integrated in the antenna is around 300μm wide and the size of a silicon lens can be up to some centimetres in radius.
Moreover, for the device to work optimally, the photomixer integrated in the antenna has to be placed precisely in the center of the lens. This might not be so easy to achieve due to the difference in size between the

lens and the photomixer and to the fact that it is not an easy task to find the center of a lens. Furthermore, the performance of the complete device is really sensitive to these misalignments, thus, little changes would ruin the directivity and the radiation pattern, changing even the placement of the focal point. This effect is shown in Fig.2.6.

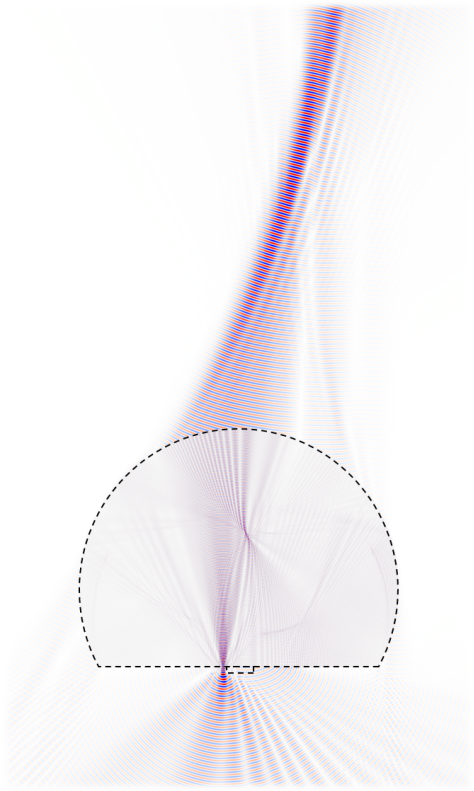

Figure 2.6: Silicon lens-antenna with a misalignment of 1mm

To conclude this chapter, an image of a real device is shown in Fig. 2.7. Taking into account the improvements that are being done in the photomixer, i.e. the use of nanocontacts and the size of the antennas employed to integrate the photomixer (explained in Sections 2.1 and 2.2, respectively), and the possibilities that they offer towards the integration in one compact device, the bulkiness that the silicon lens gives to the whole structure can be understood. Moreover, THz systems could be integrated on chip if this silicon lens was substituted, developing a whole compact system that could be fabricated at a low-cost.

Figure 2.7: Silicon lens-antenna

3 Diffractive Lenses

As it was mentioned in the Introduction (Chapter 1), the main objective of this work is to substitute the bulky silicon lens, that is commonly used in the THz photomixers to get better coupling and directivity in the generated wave. For that purpose, different possible solutions have been considered: Fresnel zone plates, phase shifted lenses and photon sieves.

3.1 Fresnel Zone Plate

In comparison with, for instance, the Fresnel lens that works by the refraction of the rays, Fresnel Zone Plates (FZP) work by interference or diffraction. A FZP is formed by concentric circular rings that alternate between opaque and transparent, placed on a transparent flat plate. The rings, or Fresnel zones, are separated in a way that the light that crosses the transparent zones interferes constructively at the focal point. This can be better appreciated in Fig. 3.1, where a side and a top views of a FZP are illustrated. Also the normal use as a lens is seen here, where the source is placed at the focal point of the plate.

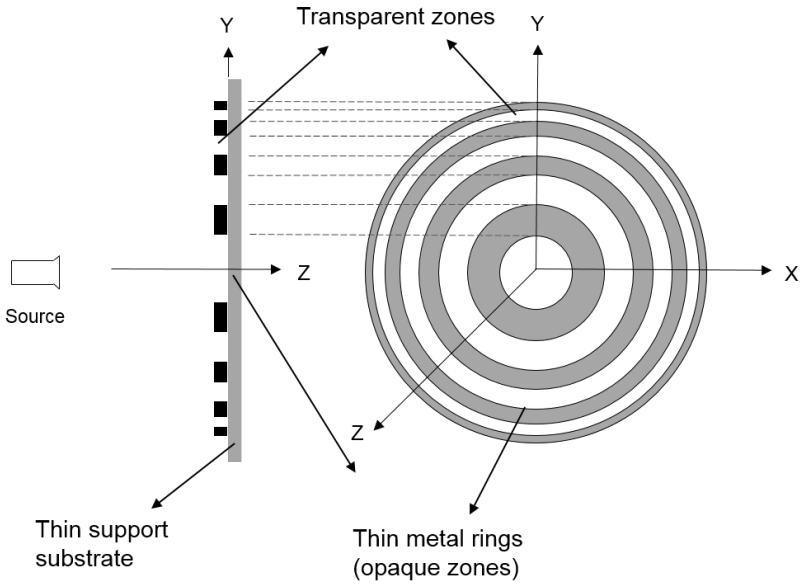

Figure 3.1: FZP (left) side view and (right) top view [10]

To derive the design equations of a FZP [10], let's consider a source on the same plane as the FZP but at a distance r from the center of it. The optical path length l between the source point and the focal point and the optical path length l_0 between a source point at the center of the FZP and the focal point are given, respectively, in the equations 3.1 and 3.2, and illustrated in Fig. 3.2.

$$l = \sqrt{r^2 + f^2} \tag{3.1}$$

$$l_0 = f \tag{3.2}$$

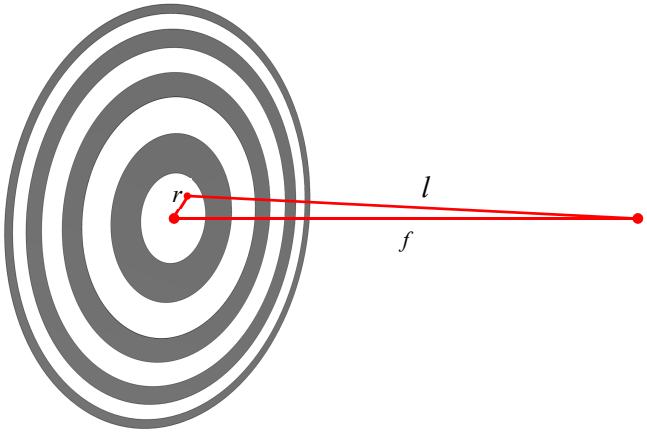

(a) Distance to any point l .

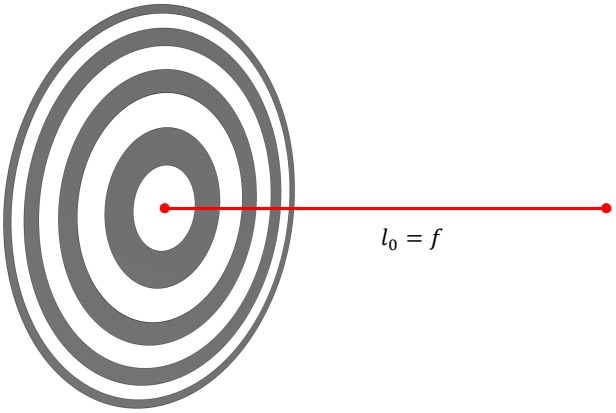

(b) Distance to the center l_0 .

Figure 3.2: Distances from the focal point f to the FZP [10]

To locate source points that will interfere constructively at the focus it is required that the optical path lengths $(l - l_0)$ differ by not more than $\lambda/2$:

$$l - l_0 < \frac{\lambda}{2} \tag{3.3}$$

Source points satisfying this criterion define the first Fresnel zone, i.e. the green area from Fig. 3.3.
As the source points move towards the outer part of the FZP, the distance to the center $l - l_0$ increases beyond $\lambda/2$. The sources with optical path lengths satisfying:

$$\frac{\lambda}{2} < l - l_0 < \lambda \tag{3.4}$$

will be part of the second Fresnel zone (Fig. 3.4) and will interfere destructively at the focus with the sources in the first zone.
Generalizing this behavior to the nth zone, the source points in it will satisfy the following expression:

$$\frac{(n-1)\,\lambda}{2} < l - l_0 < n\lambda \tag{3.5}$$

where n is an integer from *1* to N, where N is the total number of Fresnel zones in the plate.
The odd zones of the plate will interfere constructively whereas the even zones will interfere destructively.

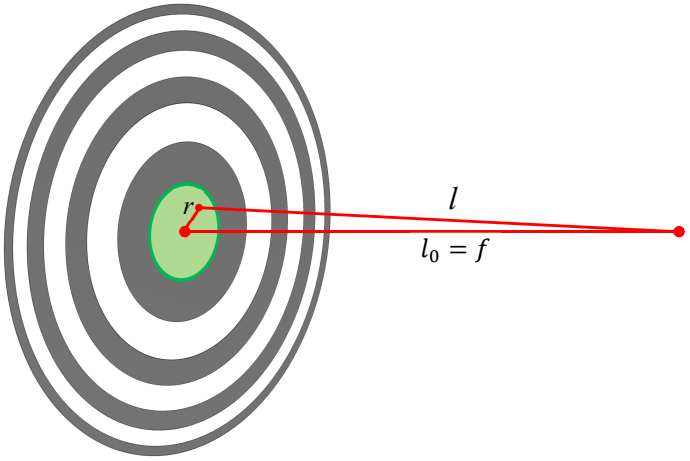

Figure 3.3: First Fresnel zone highlighted in green [10]

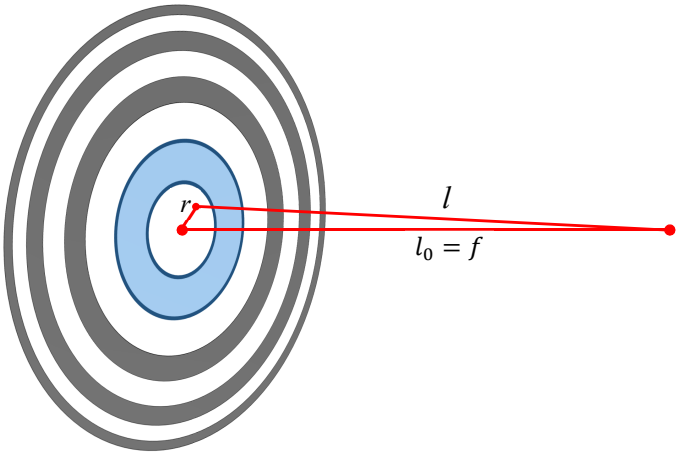

Figure 3.4: Second Fresnel zone highlighted in blue [10]

It can be noted that a FZP can start either with a transparent or an opaque zone and the effective lens will be the same.
Therefore, optical path lengths differences satisfying the following expression will delimit the boundaries of the zones:

$$l - l_0 < \frac{n\lambda}{2} \tag{3.6}$$

Rewriting the expression in terms of the source point's radii:

$$\sqrt{f^2 + r_n^2} - f = \frac{n\lambda}{2} \tag{3.7}$$

Solving 3.7 for r_n, the radii of the zones can be obtained by the expression in 3.8, where the wavelength λ and the focal distance f are taken into account.

$$r_n = \sqrt{n\lambda\left(f + \frac{n\lambda}{4}\right)} \tag{3.8}$$

In order to calculate the zones of the FZP, the first step would consist of calculating the minimum number of zones required to satisfy the design specifications, which will include again the frequency (or wavelength λ),

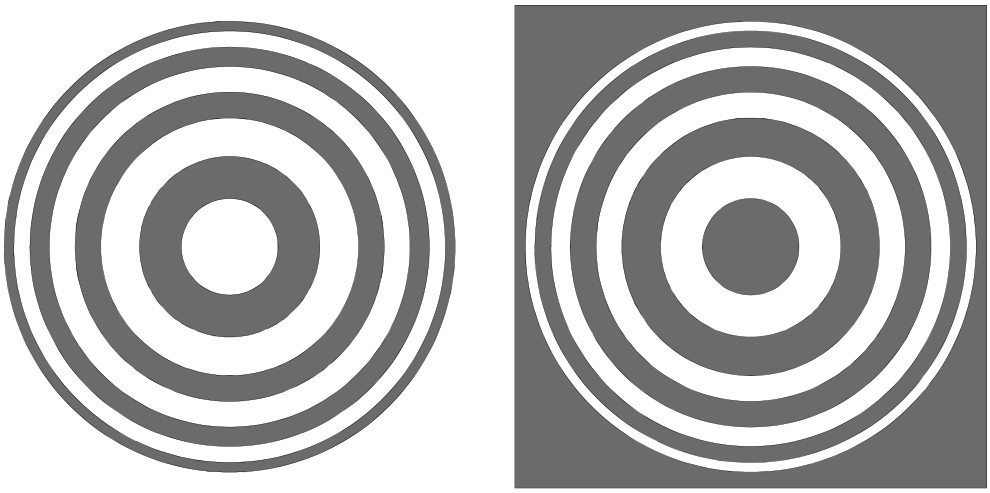

Figure 3.5: Fresnel zone plates starting with transparent or opaque zones [10]

the resolution (ω) and the focal distance (f). All these parameters are considered in the following equation:

$$N = \frac{\lambda f}{4w^2} \tag{3.9}$$

Taking a look into Eq. 3.8 and 3.9 it can be seen that the focal length of the FZP depends on the wavelength of radiation, whereas in the Fresnel lens it was independent of the frequency. However, it does not mean that the FZP is not working any more if a different frequency from the one used to design is radiated, but simply a change in the focal distance will be experienced. Another relation that can be extracted from these equations is that if resolution wants to be increased, then the number of zones has to be also higher. Therefore, a compromise between the size and the resolution must be taken.
Since half of the radiation is reflected backwards due to the opaque zones (metal rings), a big amount of energy does not propagate towards the focal plane. Thus, in comparison with the commonly used silicon lens, the efficiency becomes lower. Also, if the illuminating efficiency is low, i.e. the incident wave does not cover completely the plate, the focal point will be compromised.
Although FZPs have some disadvantages compared with dielectric lenses, they appear to be a good solution in some X-ray applications like microscopy due to their flatness, fabrication simplicity and capability of high resolution focal points.

3.2 Phase Shifted or Grooved Lens

The main disadvantage with FZPs is that since the part of the wave that does not propagate is reflected back, half of the radiated power is already lost due to this reflection. Another method to achieve a diffraction lens without using reflecting materials to stop the destructive contribution of the wave is the phase shifted or grooved lens [11].
Thus, instead of blocking the part of the input light that would be destructive at the focal point, what can be done is groove the surface of the lens in a number of steps p, achieving a phase shift of the wave that will lead to a constructive addition at the focal point. The height of these steps will be given by:

$$t_1 = \frac{\lambda_0}{p\,(n-1)} \tag{3.10}$$

And the total thickness of the lens by:

$$t_1 = \frac{(p-1)\,\lambda_0}{p\,(n-1)} \tag{3.11}$$

Both equations 3.10 and 3.11 depend on the desired number of steps p, the wavelength λ_0 and the permittivity of the dielectric used for the lens. Fig. 3.6 shows the shape for a two step ($p=2$) grooved-FZP lens.

Figure 3.6: Two-step grooved-FZP lens

3.3 Photon Sieves

The smallest focal point that Fresnel zone plates can achieve is limited by the outermost radius of it. Photon Sieves (PS) appear then as an alternative for some applications in the range of X-rays as well. The structure of a PS consists on a large set of pinholes placed strategically over the Fresnel zones, reaching spot sizes smaller than the diameter of the smallest pinhole [12].

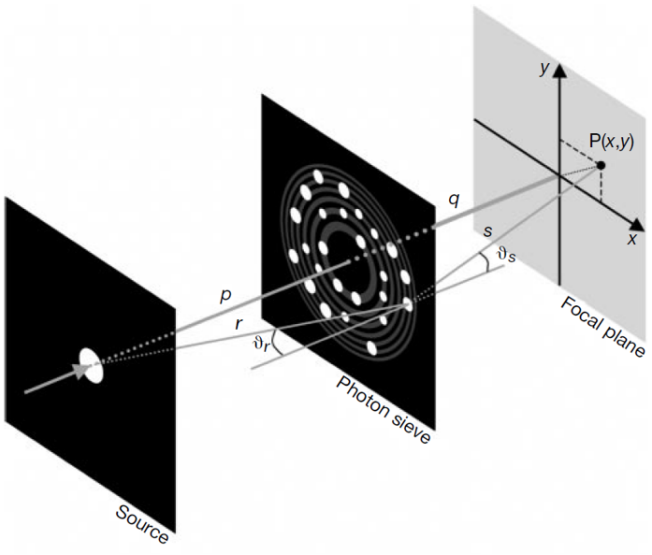

Figure 3.7: Working principle of a photon sieve [12]

The structure of a general PS is shown in Fig. 3.7, where the pinholes (white holes) are placed randomly on the metal surface (black surface). To obtain a focal point, the pinholes have to satisfy a simple condition: the optical path length between the source through the center of the pinholes to the focal point has to be an integral number of λ. Therefore, the pinholes have to be centered at distances r_n from the optical axes given by:

$$\sqrt{r_n^2 + p^2} + \sqrt{r_n^2 + q^2} = p + q + n\lambda \tag{3.12}$$

where λ is the wavelength and n is a postive integer. The distribution followed to choose the integers n and the position of the pinholes can yield to aberration correction.
Regarding the diameter of the pinholes d, they should cover only the constructive interference zone, so the light coming from all parts of the pinhole interfere constructively at the focal point. If the diameters are bigger than this area, they will also partially contribute to the focal point even though a part of the light contributes destructively. As long as the biggest area covered is constructive, a focal point will be achieved.
Furthermore, one of the main advantages of using photon sieves instead of FZP is that higher orders of diffraction and secondary maxima are avoided. This is represented in the following image:

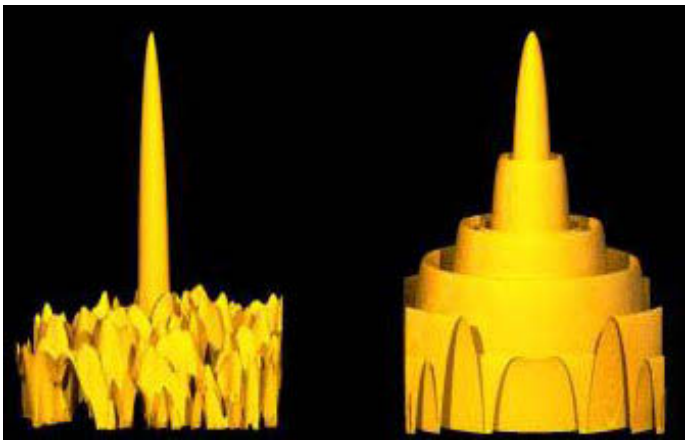

Figure 3.8: Radiation diagram of (left) a photon sieve and (right) a FZP [13]

4 Moth-Eye Structure

Anti-reflective layers are employed in many different technologies and frequency ranges in order to improve the coupling or the impedance matching of the waves at the interfaces of two materials with different refractive indexes. Examples go from using some material layers with different refractive indexes to make the coupling progressive, to more complicated structures, like the one explained in this chapter: moth-eye structures.
The idea is inspired by the eyes of some insects like moths, butterflies or flies that are less sensitive to reflectance, which increases the sensitivity of their visual system . This is due to a pyramidal structure placed on the surface of their eyes (Fig.4.1a) that acts as a grating that, from the perspective of the incident wave, cannot be resolved (Fig.4.1b). Therefore, the refractive index that is seen by the wave has a progressive value between the refractive indexes of the media it is crossing, achieving a better result than with a thin layer, as is it illustrated in Fig.4.1c.

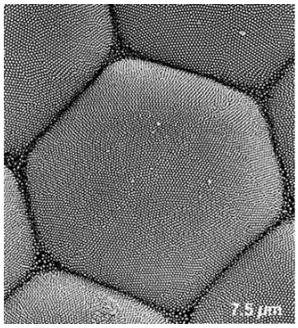

(a) Eye of a moth [14]

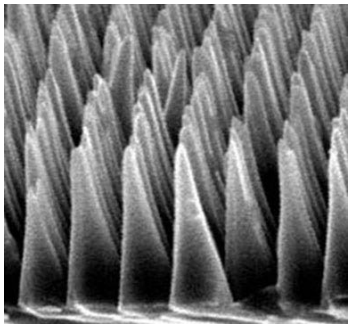

(b) Example of moth-eye structure in silicon carbide [14]

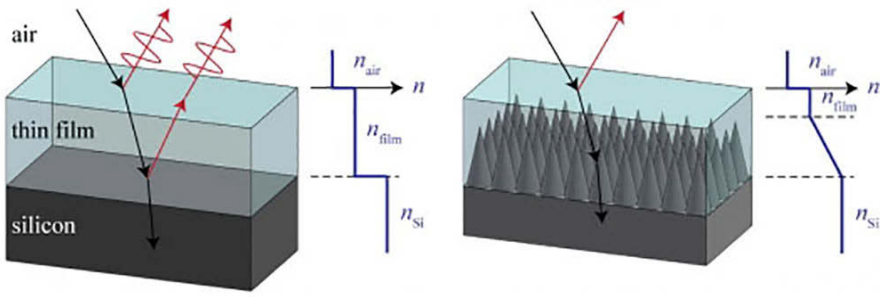

(c) Reflectange with a thin layer (left) and a moth-eye structure(right) [15]

Figure 4.1: Moth-eye structure

Moreover, they present some other advantages compared, for instance, with the thin layer anti-reflective solution, like the independence on polarization or on the wave incident angle, having a range that goes between $\pm 40^o$ [16].
The structural period of the moth-eye anti-reflective structure, which can also work in the THz range, is determined by the shortest wavelength of the spectrum, whereas the structural depth is specified by the largest wavelength of the spectrum. When translating this to the whole THz range, a ratio of 100 (from 10 μm to 1 mm) outcomes for an antireflection coating, which is neither producible nor mechanical stabile.

Thus, the moth-eye structure has to be designed for a sub-region of the spectrum and so there will be a bandwidth limit.
If the incident wave vector lies in the plane that is perpendicular to the surface and contains the grating vector, the grating period can be calculated with the following expression:

$$\Lambda = \frac{\lambda}{n_s} \tag{4.1}$$

In case of a 2D grating with modulations in x and y directions, Eq. (4.1) must be met for every single direction.
The dependence of the reflectance from the effective thickness d of a layer with a gradient refractive index and a wavelength λ was calculated by modelling the gradient layer by many layers of equal thickness with progressive increasing refractive index in [17] and is shown in Fig.4.2.

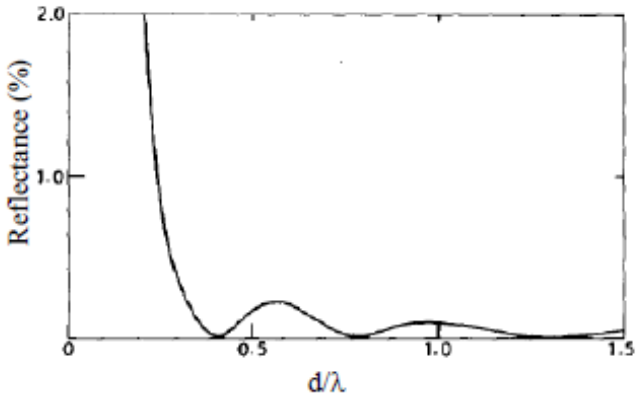

Figure 4.2: Dependence of the reflectance from d/λ

The reflectance index falls to a first minima at:

$$\frac{d}{\lambda} = 0.4 \tag{4.2}$$

By increasing d/λ the value never reaches one of the sharp boundary. For $d >> \lambda$ reflectance is effectively zero.

5 Finite Difference Time Domain Method: Meep Software

The simulation of any device that wants to be implemented is strictly necessary nowadays. Therefore, choosing a suitable solving method depending on the characteristics of the device, the frequency range and the features that have to be tested must be a precise task and it appears to be one of the most important ones at the beginning of any work.
The main solving method that has been chosen for this particular work is the Finite Difference Time Domain (FDTD) Method, which solves the coupled Maxwell's curl equations directly in the time domain by using finite time steps over small cells in space. The method reduces the differential equations to difference equations that can be solved by sets of simple equations. It alternates between the electric and magnetic fields solved at locations a half-step apart because central differences are used to approximate derivatives. Moreover, since each cell is allowed to be implemented with different materials, complex structures can be simulated. The FDTD method can be applied to many different electromagnetic problems including antennas, like in this case, but also optics, biological interaction with electromagnetic waves and many more [18].
One software that uses the FDTD method and that is the one that has been used for this work, is the MIT's open-source Meep Software. Meep runs on a Linux OS, it is programmable in python, unitless and does not have a graphical interface, therefore, every resulting image or postprocessing has to be generated by the user. Something that is important to mention about the FDTD method is that it is limited by the speed and space of the processor where the simulation is running because the files generated tend to increase their size really easily. Therefore, high frequency simulations with different orders of sizes in the structure will require really high resolutions (large mesh), memory space and time.
In Fig.5.1 a scheme of the process to perform a simulation in shown. The first step is always to generate the code in python, where the structure to simulate is generated from simple geometrical forms and the simulation characteristics are specified. Afterwards, it has to be run from the terminal and by means of some postprocessing of the generated files (.h5 type files), results can be obtained, like images of the fields. One of the reasons why this method is used instead of the Finite Integration Technique (FIT), which is used by CST Studio, is because it discretizes the space to numerically solve the electromagnetic field problems and, in this case, it might not be accurate enough [19]. However, even though the FDTD is the main technique used in this work, some simulations have also been run in CST Suite Studio in order to compare and obtain some other results (see Section 7.2).

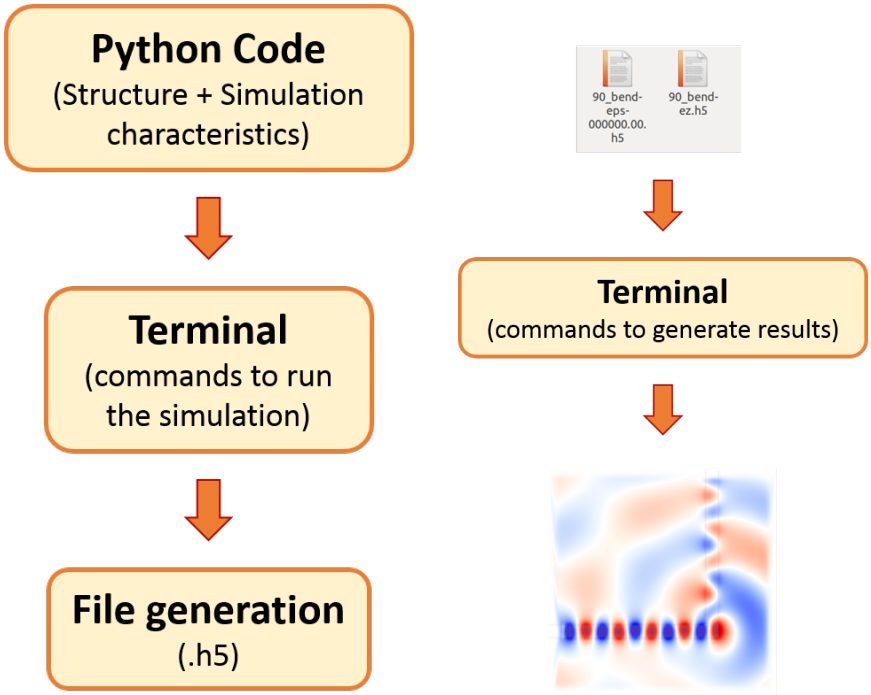

(a) Generation of a simulation (b) Postprocessing

Figure 5.1: Steps in Meep software to generate a simulation and obtaining results

6 Mounted Lens-Antenna Designs

This chapter will contain the first antenna designs, which will consist of mounted FZP lenses on top of the LTG-GaAs made out of different materials: section 6.1 with Teflon and sections 6.2 and 6.3 with silicon, including this last one a moth-eye structure.
Some of the parameters are common for all the designs that will be explained along this chapter, like the frequency, that had to be delimited from the whole THz range in order to be able to optimize the antenna, or the resolution of the FZP. These general parameters are in Table 6.1.

Frequency	1THz
Wavelength (λ_0)	0.3mm
Focal length (f)	15mm
Resolution (w)	150μm

Table 6.1: General design parameters

The substrate that will be used for the photomixer and the antenna will be LTG-GaAs due to its characteristics explained in Chapter 2. The electrical permittivity and refractive index, together with the thickness and length of the wafer are specified in Table 6.2 and correspond to a standard LTG-GaAs wafer.

ε_r	12.97
n	3.59
Thickness	350μm
Length	1.5mm

Table 6.2: LGT-GaAs characteristics

Regarding the simulations that will be shown along the chapter, they have all been performed in Meep with a source of width 0.3μm, at the frequency specified in Table 6.1 and placed at the bottom of the substrate, i.e. at 350μm (thickness of the wafer) from the FZP.

6.1 Teflon FZP Lens-Antenna Design

The first presented design consists of a FZP teflon lens attached to the substrate (LTG-GaAs). The grooved lens type explained in Section 3.2 has been applied here, so a typical lens could be transformed into a planar lens, using a FZP.
For the design of the teflon FZP lens, the first that needs to be calculated is the number of zones that are required for the general specifications listed in Table 6.1. In order to do so, Eq. 3.9 is used with λ in the substrate that will be given by Eq. 6.1. The resulting wavelength for teflon, which has a refractive index n = 1.44 [8], is of λ = 208.33μm. Thus, the minimum number of zones obtained is N = 35. Since the best behaviour of the FZP is obtained when the first Fresnel zone is a constructive area, N = 36 zones will be used here.

$$\lambda = \frac{c_0}{\lambda_0 \sqrt{\varepsilon_r}} \tag{6.1}$$

The following step, once the number of zones has been determined, is to calculate the radii of the Fresnel zones. Applying Eq. 3.8, the values from Table 6.3 are obtained (in μm).

r_1	1770.833	r_{19}	7955.633
r_2	2508.666	r_{20}	8175.590
r_3	3077.768	r_{21}	8391.076
r_4	3560.002	r_{22}	8602.426
r_5	3987.012	r_{23}	8809.939
r_6	4375	r_{24}	9013.878
r_7	4733.570	r_{25}	9214.482
r_8	5068.969	r_{26}	9411.964
r_9	5385.527	r_{27}	9606.516
r_{10}	5686.393	r_{28}	9798.313
r_{11}	5973.938	r_{29}	9987.514
r_{12}	6250	r_{30}	10174.263
r_{13}	6516.039	r_{31}	10358.693
r_{14}	6773.237	r_{32}	10540.925
r_{15}	7022.564	r_{33}	10721.073
r_{16}	7264.832	r_{34}	10899.239
r_{17}	7500.723	r_{35}	11075.518
r_{18}	7730.823	r_{36}	11250

Table 6.3: Teflon FZP radii values

Finally, an etching depth of $\frac{\lambda}{2} = 104.17\mu$m is needed for a $p = 2$, according to Eq. 3.10. With all these parameters, the device from Fig. 6.1a is obtained.

(a) Transversal cut

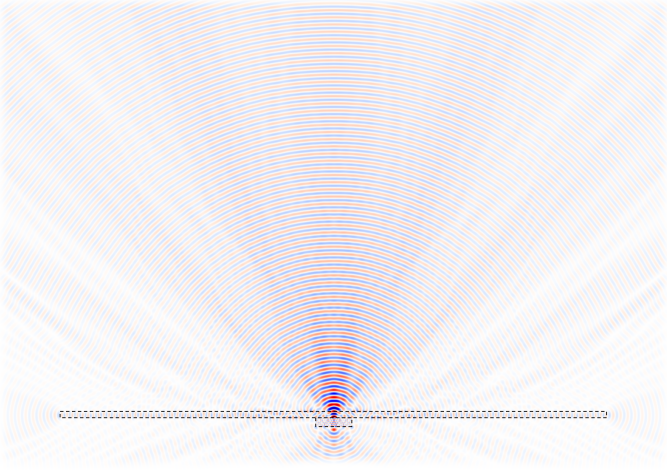

(b) Electric field

Figure 6.1: Results of the teflon FZP lens-antenna design

The simulation run in Meep gave the resulting electrical field showed in Fig. 6.1b, where the size of the cell is of 28.56x20 mm. It is seen in the simulation that some directivity is achieved but not as much as would be needed. In fact, two main beams are generated and, when compared with the normal substrate without any kind of focusing system, the difference does not appear to be big.
The total thickness of the lens had to be, according to Eq. 3.11, of $\frac{\lambda}{2}$ but a base was needed to hold the FZP.

Therefore, before choosing one final value for the thickness, a study has been done for a base of thickness $\frac{\lambda}{2}$, λ and 2λ. The structures with their respective resulting fields are shown in Fig.6.2.

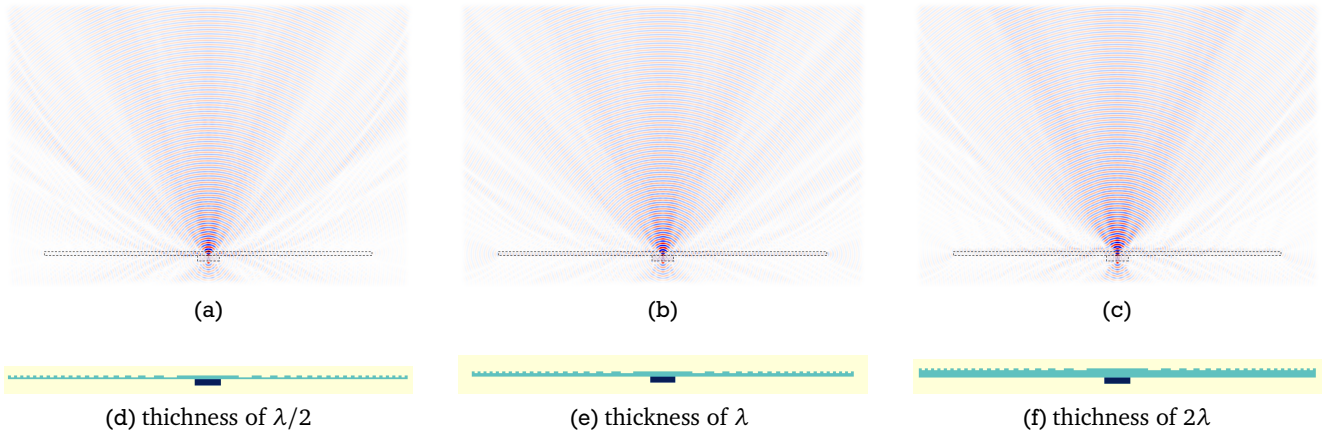

(d) thichness of $\lambda/2$ (e) thickness of λ (f) thichness of 2λ

Figure 6.2: Electric fields for different thicknesses of the teflon FZP's base

There is a big difference that can be appreciated between the fields of $\lambda/2$ and λ in terms of cleanness in the output beam. However, when the results between λ and 2λ are compared, the difference in the shape of the beam is almost imperceptible. Thus, a base of thickness λ for the FZP has been chosen.
The here presented teflon FZP mounted on top of the LTG-GaAs substrate is still a very big device. Having in mind that one of the main objectives of this work was to reduce the size of the emitter in a THz system, some other options have been considered, like changing the material used for the FZP in order to reduce the size of it.

6.2 Silicon FZP Lens-Antenna Design

A similar device to the one from the previous section has been designed here. In this case, the teflon lens has been substituted by a silicon lens but, again, a planar grooved FZP has been used, avoiding the bulkiness of the commonly used device from Section 2.3.
In this case, since the material has a different refractive index, or electrical permittivity, the characteristics of the FZP change and thus, the number of zones and radii have to be recalculated.
According to Eq. 6.1, the wavelength in silicon, which has a refractive index in the THz range of $n = 3.43$ [8], will be $\lambda = 87.46\mu$m. Using again Eq. 3.9, for the just calculated wavelength λ and the focal length and resolution established as general parameters in Table 6.1, a minimum number of Fresnel zones $N = 15$ is obtained. Since a better performance is achieved when starting with a constructive area, a number of $N = 16$ will be used here. Therefore, according to the Eq. 3.8, the radii values obtained are the ones in Table 6.4 in μm.

r_1	1146.239	r_9	3458.684
r_2	1622.073	r_{10}	3648.394
r_3	1988.233	r_{11}	3829.216
r_4	2297.480	r_{12}	4002.354
r_5	2570.521	r_{13}	4168.765
r_6	2817.902	r_{14}	4329.225
r_7	3045.880	r_{15}	4484.374
r_8	3258.531	r_{16}	4634.743

Table 6.4: Silicon FZP radii values

With this values, the structure in Fig.6.3a is obtained. Compared with the previous teflon lens design, the main difference lies in the fact that the FZP is smaller, which means already a big advantage. This is due to the fact that the wavelength in the material λ is smaller and therefore, less zones are needed.
After simulating this design in Meep, the result from Fig.6.3b is obtained in a cell of 11.59x20 mm. When compared with the previous one, whose lens was made out of teflon, it is evident that the performance is better. This is due to two facts. First of all, the refractive index of silicon is more similar to the one from LTG-GaAs (Table 6.2) and therefore, the coupling is done easier at the interface between the substrate and the air. With respect to the second reason, since the source is situated at only 350μm from the lens, i.e. the thickness of the substrate, not all the FZP is directly illuminated by the input wave. Thus, the smaller the FZP is, i.e., less zones and smaller radii it has, the more area will be illuminated and the efficiency will be bigger.

(a) Transversal cut

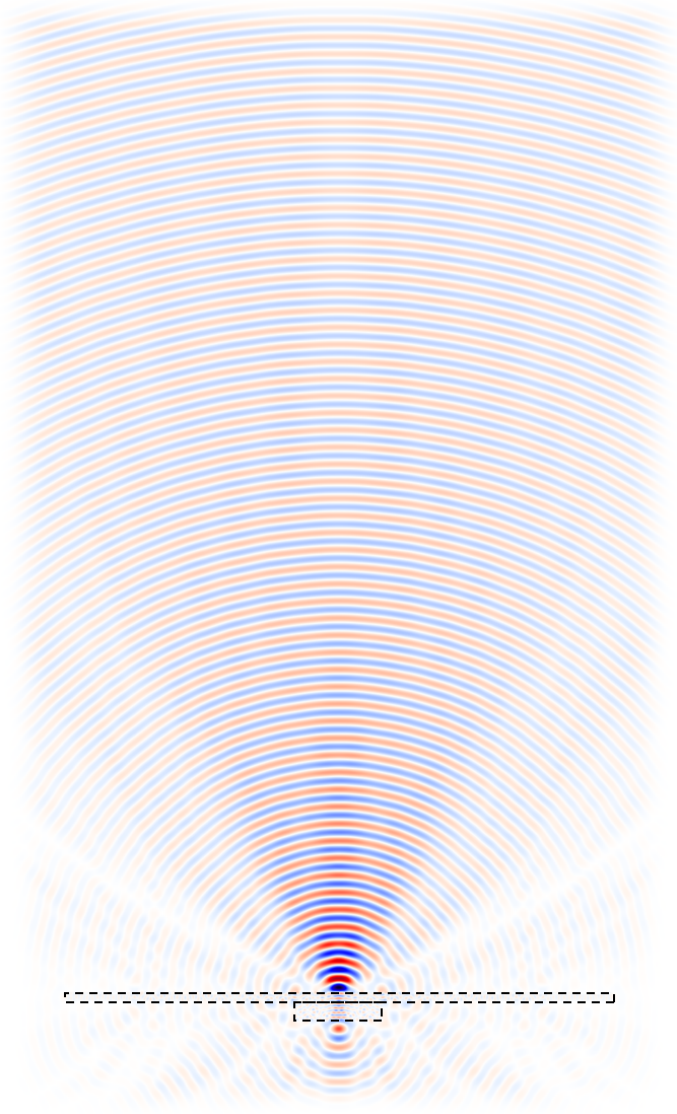

(b) Electric field

Figure 6.3: Results of the silicon FZP lens-antenna design

6.3 Silicon FZP Lens-Antenna Design with a Moth-Eye Structure

To finalize with the mounted lens designs, some improvement has been done on the design from Section 6.2, adding a moth-eye structure on top of the silicon FZP. The purpose of it is to try to improve the coupling at the interface between the air and the silicon, making it as a progressive change in the refractive index, as was explained in Chapter 4.
According to the Eq. 4.1, and Eq. 4.2, the values for the grating period and the thickness that are needed for the pyramids of the moth-eye structure in the interface silicon-air can be found in Table 6.5.

Grating Period (Λ)	25.5μm
Thickness (d)	34.99μm

Table 6.5: Size of the pyramids of the moth-eye structure

This structure has been tested in different positions of the FZP, including covering the whole FZP, only on top of the not etched rings and only on the first Fresnel zone (central ring). These different designs are shown in Fig. 6.4 and the best performance was obtained for the case in which the pyramids of the moth-eye structure were placed only on top of the central ring, i.e. Fig.6.4c.

(a) All over the FZP

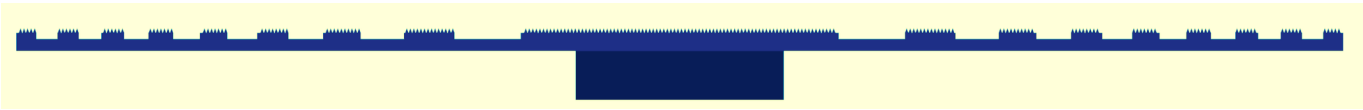

(b) Only on top of the not etched rings

(c) Only on the first Fresnel zone (central ring)

Figure 6.4: Different positions of the moth-eye structure on the silicon FZP lens-antenna

This design will have the same appearance like the one in the previous section, because the needed FZP is the same, but with the moth-eye structure placed on top. After the new parameter calculations for the pyramids, the whole structure will look like Fig.6.5.
With the structure from Fig.6.5, the 2D simulation from Fig.6.6 was obtained. The field distribution shows a better performance of the silicon FZP compared with the one from Section 6.2 due to the fact that a better coupling between the FZP and the air is achieved.
The main disadvantage of all the designs presented along this chapter is that a lens has to still be mounted on top of the substrate and, therefore, important misalignments can occur easily during the implementation. Thus, other options will be studied in the following chapter.

(a) Transversal cut

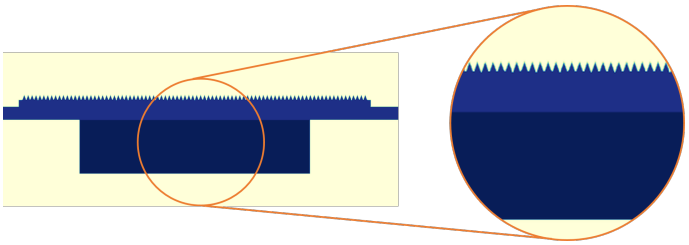

(b) Zoom centered in the moth-eye structure

Figure 6.5: Transversal views of the silicon FZP lens-antenna with a moth-eye structure

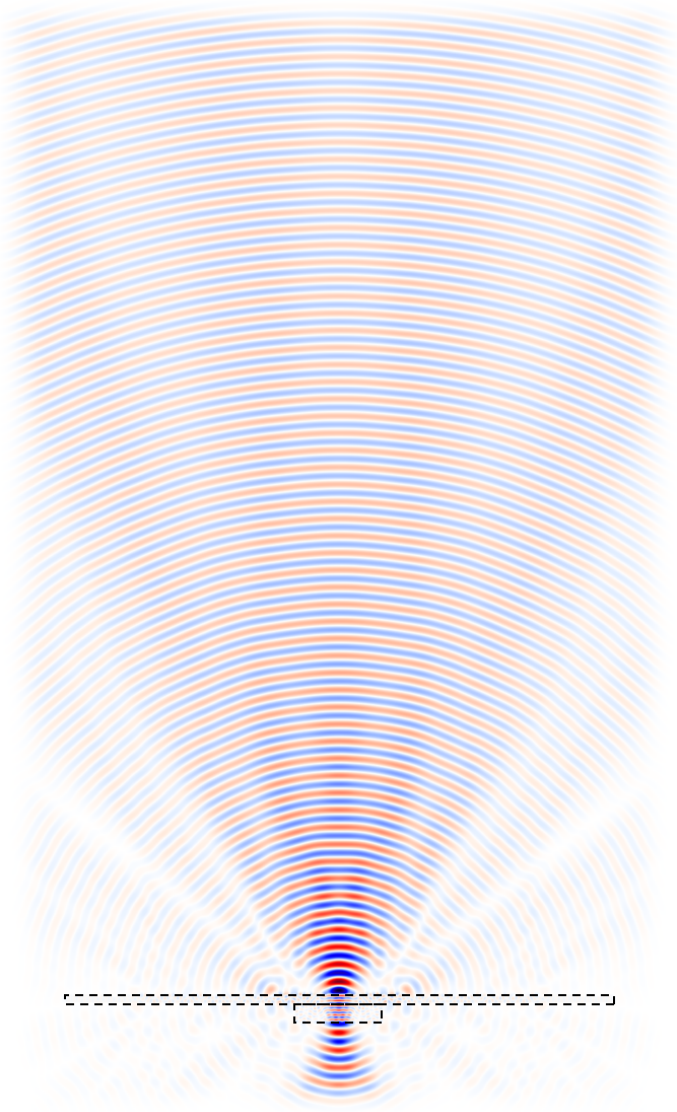

Figure 6.6: 2D simulation of the silicon FZP lens-antenna with a moth-eye structure

7 Integrated Lens-Antenna Design

In this chapter the design of the integrated FZP lens-antenna is presented. As opposed to the previous designs from Chapter 6, no lens is mounted in this case on the LTG-GaAs substrate, but the FZP is directly etched on top of it. This main difference allows to implement the device in only two simple steps of normal optical lithography and avoids one of the main problems that appeared with the commonly used silicon lens, which is the misalignment between the lens and the photomixer. In section 7.1 the basic design will be explained and in sections 7.2 and 7.3 some modifications will be done in order to improve the performance of the antenna.
The substrate that will be used for the photomixer and the antenna will be the same as for the previous designs in Chapter 6: LTG-GaAs. The properties of it can be found in Table 6.2, although, in this case, the length of the wafer and, therefore, from the whole device, will be defined by the diameter of the biggest Fresnel zone.
Since the FZP will be etched on the substrate itself, the wavelength in the substrate must be calculated. According to Eq. 6.1 and the electrical permittivity from Table 6.2, the value from Table 7.1 is gotten. This value will be used for all the designs of this chapter.

Wavelength (λ)	83.3μm

Table 7.1: Wavelength in the substrate

Regarding the simulations that have been performed in Meep along this chapter, all of them have been done with a source of width 0.3μm, at the frequency of 1THz, as was specified in Table 6.1, and placed at the bottom of the substrate, i.e. at 350μm (thickness of the wafer) from the FZP. Moreover, all the sizes of the simulation cells are of 11x20 mm.

7.1 Integrated FZP Lens-Antenna in LTG-GaAs

As it was done also in the previous designs, the first step to design the FZP is to calculate the number of rings that are needed. According to Eq. 3.9, the resolution specified in Table 6.1 and the wavelength from Table 7.1, the number of zones needed by this FZP is $N = 14$.
Regarding the radii of the lens, they are calculated according to Eq. 3.8, getting the values in Table 7.2, where all the values are expressed in μm.

r_1	1118.594	r_8	3179.178
r_2	1583.027	r_9	3374.341
r_3	1940.146	r_{10}	3559.306
r_4	2241.836	r_{11}	3735.586
r_5	2508.179	r_{12}	3904.360
r_6	2749.465	r_{13}	4066.560
r_7	2971.806	r_{14}	4222.945

Table 7.2: FZP radii values

Since the FZP is etched on top of the LTG-GaAs, an etching depth is needed. As it was done for the other

designs, the phase shifted lens type equations are used here to get the etched depth on the surface of the substrate. Again, if a two-level etching is performed ($p=2$) and Eq. 3.10 is simplified, the etching depth is given by:

$$\frac{\lambda}{2} = 41.65\mu m \tag{7.1}$$

A transversal cut of the resulting structure is shown in Fig. 7.1a and a 3D image of the top of the device in Fig. 7.1b, so a better perspective of it can be established.

(a) Transversal cut

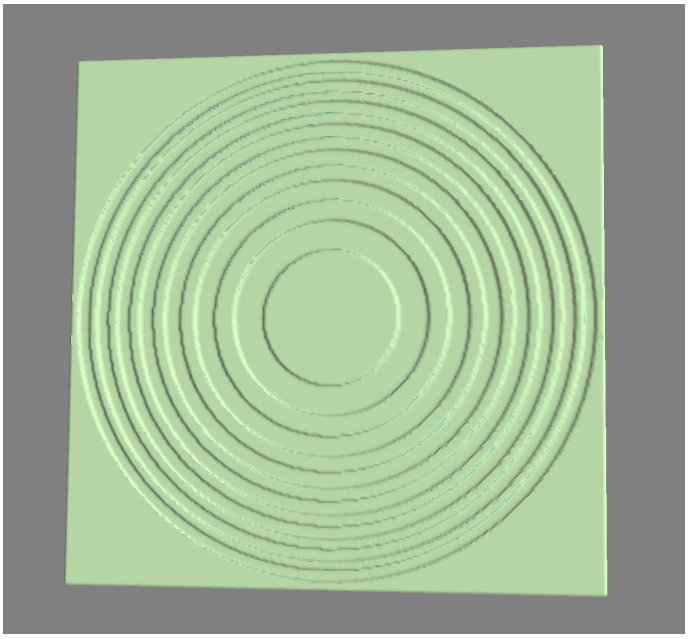

(b) 3D view

Figure 7.1: Different views of the integrated FZP lens-antenna design

This structure has been simulated in 2D in Meep in order to analyze the field distribution, which is shown in Fig.7.2. The size of the cell, as was specified above, is of 11x20 mm and the focal point should be at a distance from the device of around 15mm. However, the rays collimate at a point that is situated much closer to the device. This is, again, because since the source is not situated at a distance far enough from the FZP, it is not completely illuminated by the input wave, and therefore, the focal point appears in a different position than the theoretical or specified one. Despite this change in the focal distance, directivity is still accomplished without the need of an external or mounted lens.

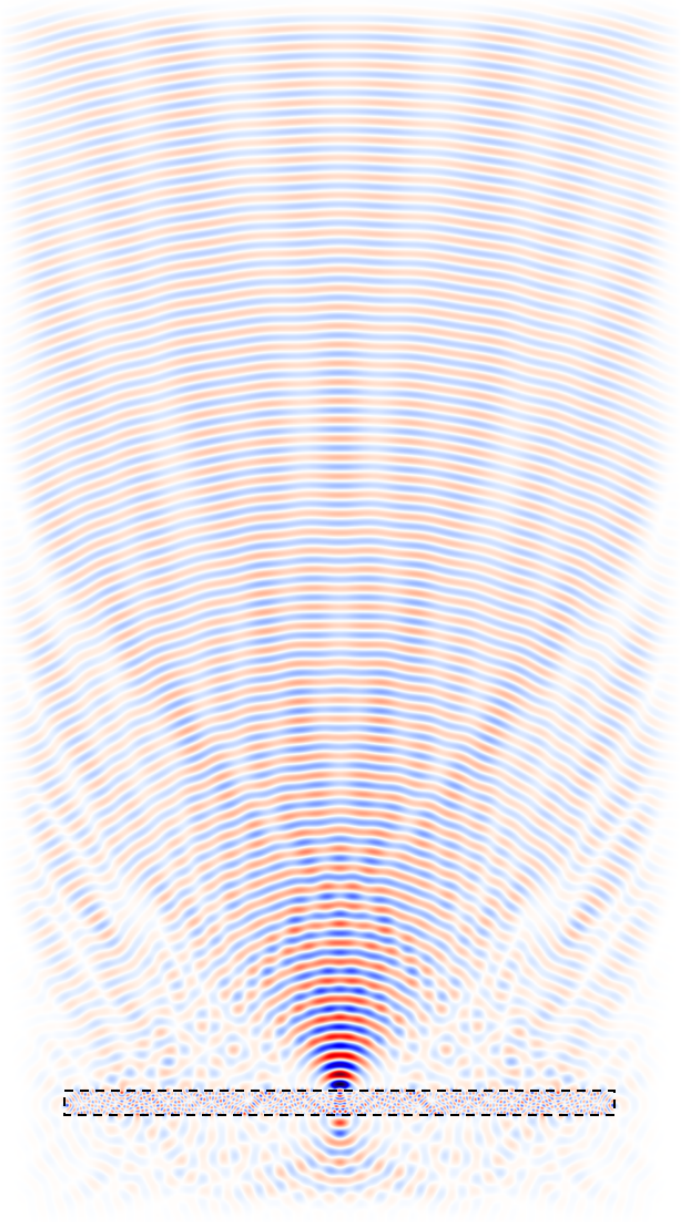

Figure 7.2: Electric field simulation result of the integrated FZP lens-antenna design

7.2 Integrated FZP Lens-Antenna in LTG-GaAs with Gold

In order to collimate a bigger amount of rays in the focal point by reflecting the rays that propagate backwards or stay in the substrate, some gold rings have been added to the design from section 7.1 on the bottom of the LTG-GaAs, around the photomixer integrated in the antenna. Therefore, the device will have the same appearance from the top, but with the gold elements on the bottom, as it is seen in Fig. 7.3a.
The thickness of the gold rings has been chosen to be of 85nm, according to the tables in [20]. Regarding the position, it was tested by simulations that the optimum was to have them directly under the etched zones from the top FZP.
The simulation in Fig. 7.3b shows a better performance compared with the results from Fig. 7.2 since less energy is radiated backwards, high orders of diffraction are attenuated and the focal point is sharper.

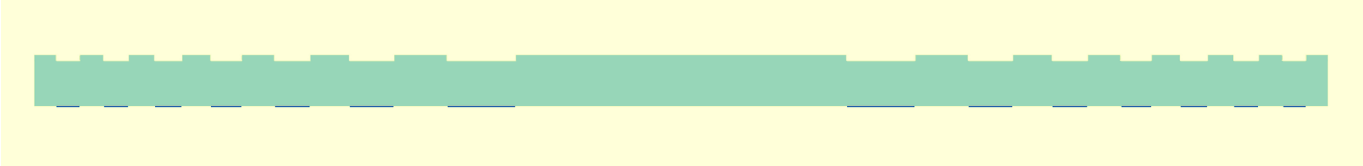

(a) Transversal cut

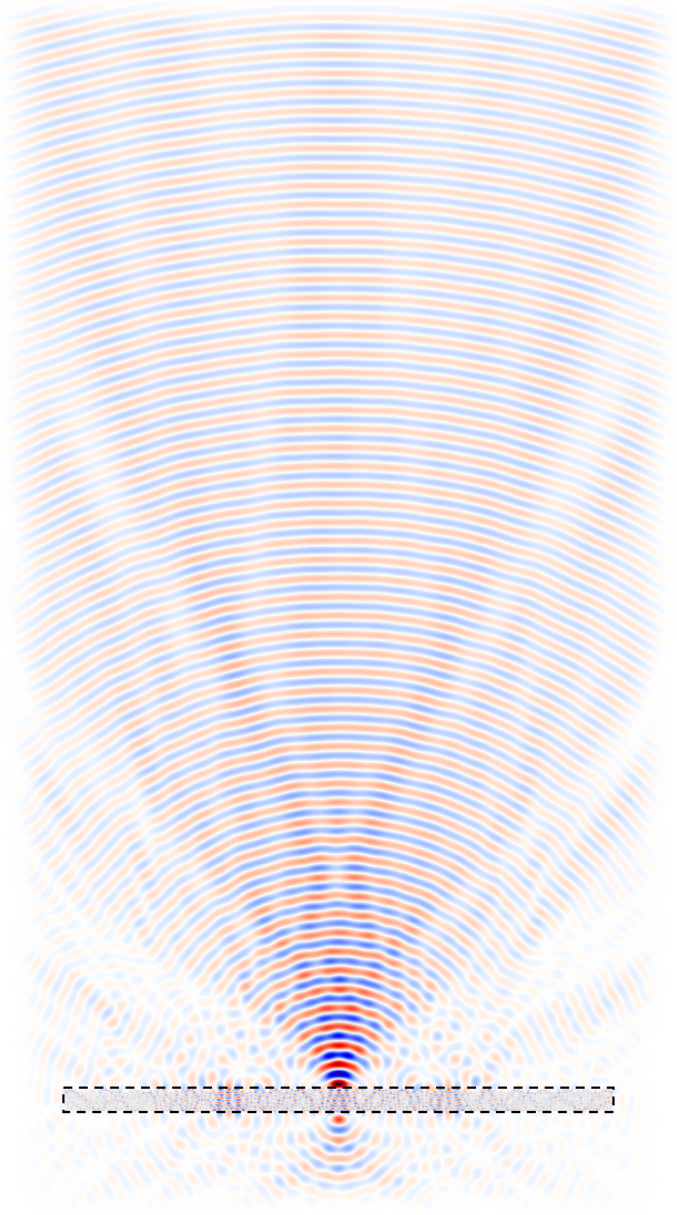

(b) Electrical field

Figure 7.3: Results of the integrated FZP lens-antenna with gold

One of the main problems with silicon lenses, a part from the bulkiness, is the misalignment between the photomixer and the lens itself, which was also mentioned in Section 2.3, when the structure of a common photomixer was explained. In this new design, where the FZP is integrated in the substrate itself, this misalignment problem becomes almost inexistent due to the different implementation process. However, if some misalignment appears, the difference in behaviour of the fields is not a big problem because a focal point is still achieved and almost at the same point as it would be for the optimal position of the source. The example in Fig. 7.4 corresponds to a misalignment that is placed inside the first ring of the FZP, which

in this case is a 1mm placement mistake of the source and would mean a big mistake in implementation.

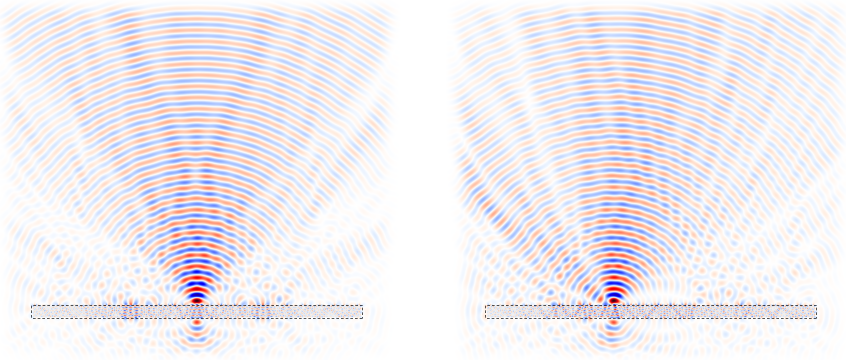

(a) Optimal position of the source (b) 1 mm disalignment of the source

Figure 7.4: Behaviour comparison between different source positions

Regarding the bandwidth, it was said in Chapter 2, that one of the design requirements was to have an antenna as broadband as possible. Therefore, and in order to compare it with the bulky and commonly used silicon lens, this design has been simulated for different frequencies. The results of some of them are shown in Fig.7.5, where it is clear that a focal point is achieved from a low frequency of 300GHz to a high frequency of 3THz, covering a big part of the THz range. However, since the design corresponds to a frequency of 1THz, the results obtained for different frequencies have different field distributions.

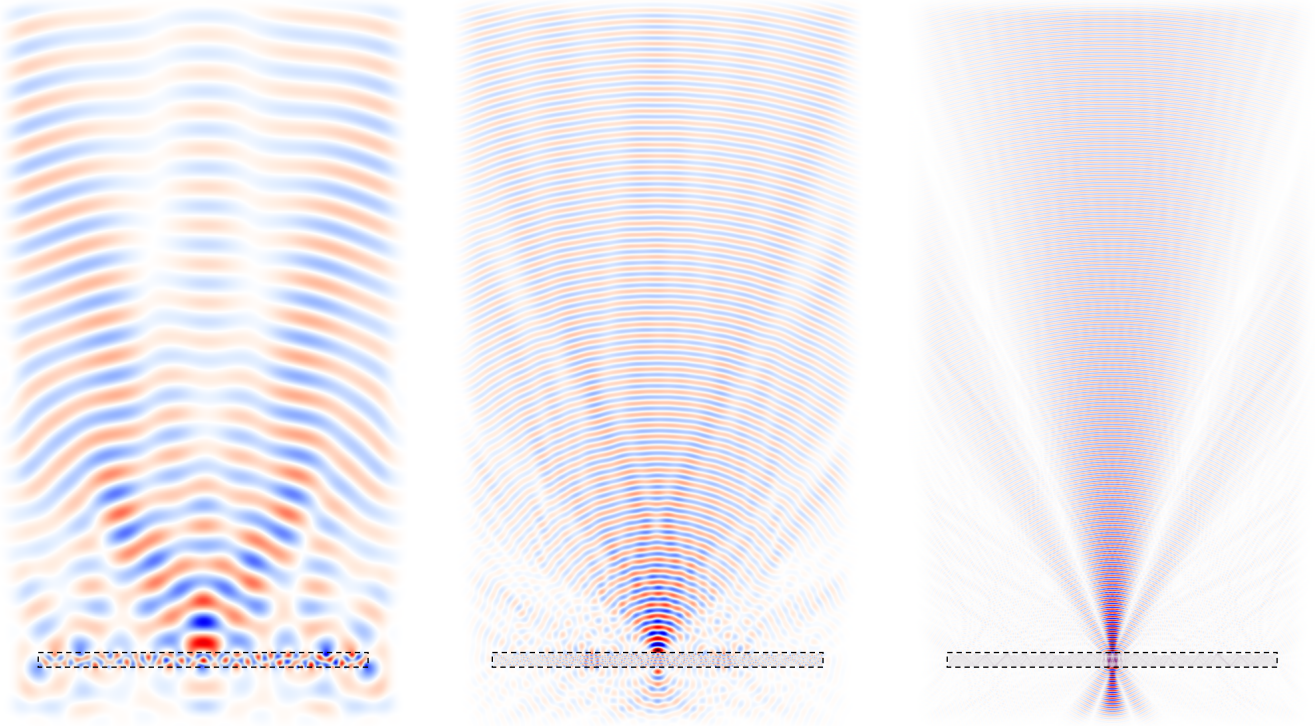

(a) $f = 300GHz$ (b) $f = 1THz$ (c) $f = 3THz$

Figure 7.5: Behaviour of the device for different frequencies

It has been decided that this design would be a suitable option to be the first one to be implemented. Therefore, it has also been tested in CST Suit Studio in order to compare the results with the different solving methods and extract some more information about the behaviour of the device. In the following figure (Fig. 7.6), both a top and bottom view are shown, so also the new added gold rings can be appreciated.

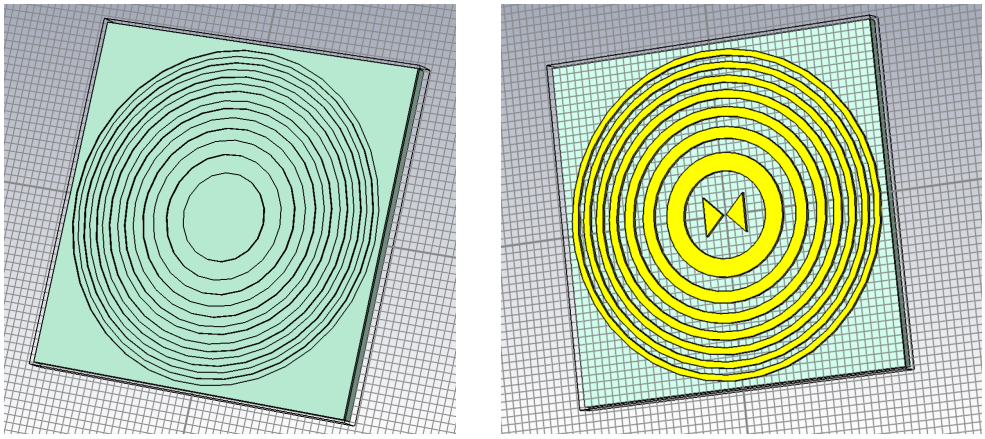

(a) Top view (b) Bottom view

Figure 7.6: 3D view of the integrated lens-antenna with gold

The S_{11} parameter obtained is shown in Fig.7.7 with a minimum at f=1067GHz, which is close to the design frequency of 1THz. Therefore, two far field monitors have been chosen for both frequencies.

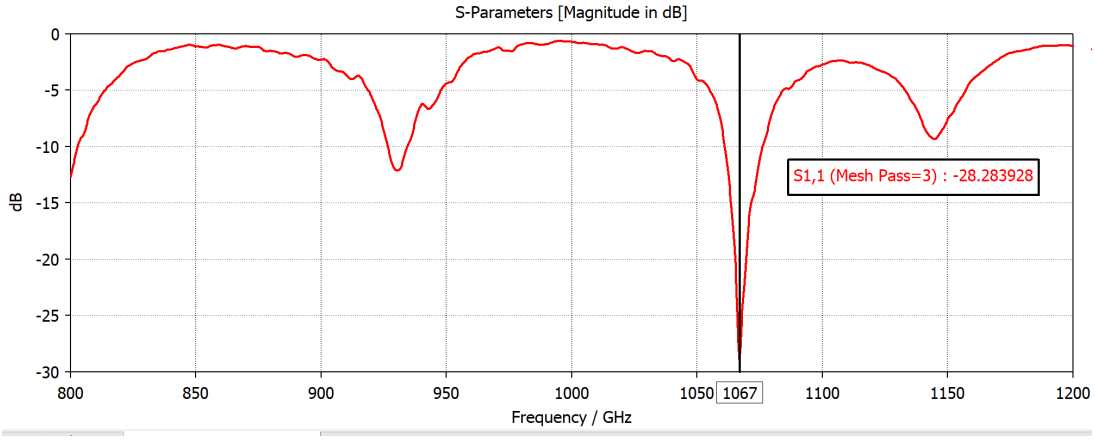

Figure 7.7: S_{11} parameter

In Fig. 7.8 the far field diagrams in 3D from the side and with a perspective are shown. It can be better appreciated that there is radiation and propagation through the LTG-GaAs substrate and that the focal point is achieved with a planar and easy-to-fabricate type of lens.
As it was expected, the results for f=1067GHz are better than the ones for f=1000GHz because a minimum in the S_{11} is obtained and thus, the least energy is propagated back to the source. This can be seen in the diagrams from Fig. 7.9, where both a 3D front view and a polar chart are shown. A maximum in radiation is obtained for the direction of 0^o for both frequencies, and the values of directivity obtained are D = 19.9dBi and D = 17.5 dBi for f=1067GHz and f=1000GHz, respectively.

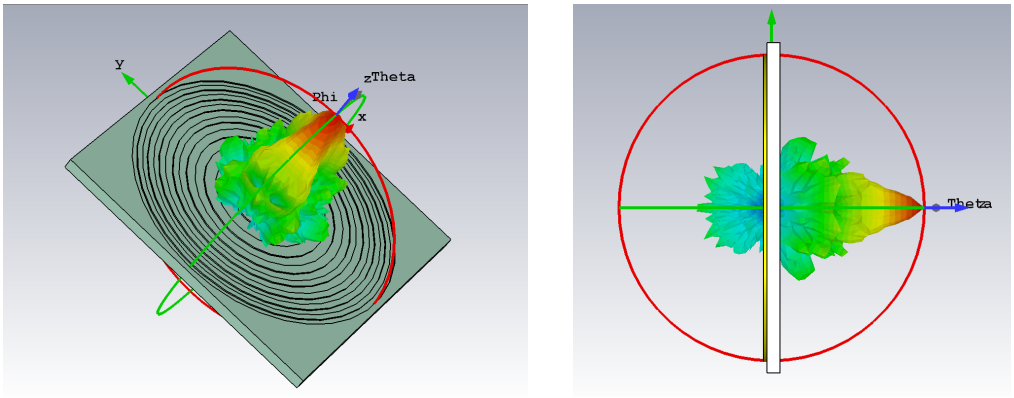

(a) Perspective view (b) Side view

Figure 7.8: 3D radiation diagrams of the integrated lens-antenna with gold

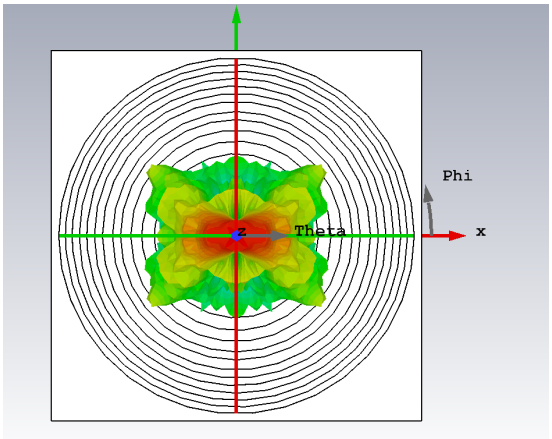

(a) 3D front view f=1000GHz

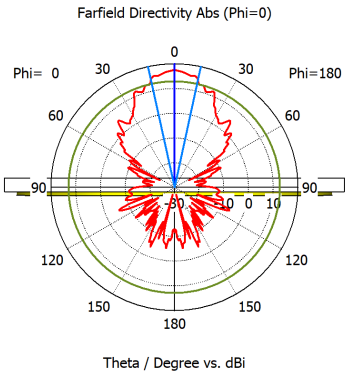

(b) Polar chart f=1000GHz

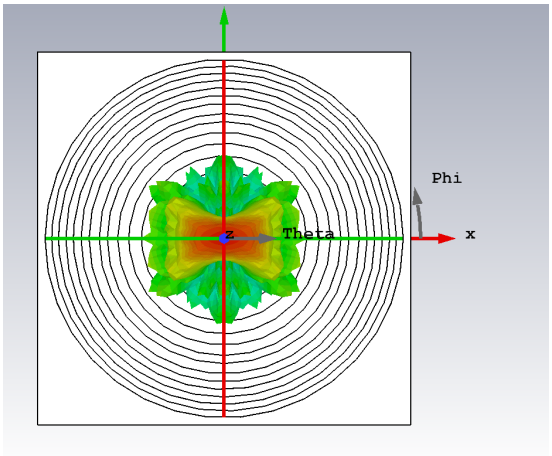

(c) 3D front view f=1067GHz

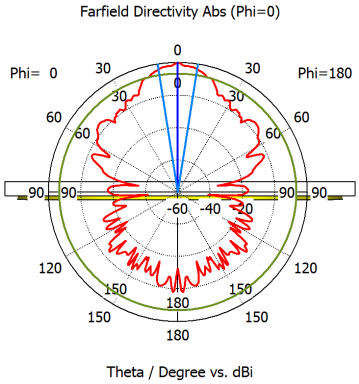

(d) Polar chart f=1067GHz

Figure 7.9: Radiation diagrams of the integrated lens-antenna with gold

7.3 Integrated FZP Lens-Antenna in LTG-GaAs with Gold and a Moth-Eye Structure

As it was done in Section 6.3 to improve the coupling at the interface silicon-air, a moth-eye structure has been added here to improve the coupling, this time, at the interface GaAs-air. The structure will be implemented again in silicon due to its ease when fabricating and its refractive index of $n = 3.43$, which is close to the one from LTG-GaAs (Table 6.2).
The values of the grating period and the thickness that are needed for the pyramids of the moth-eye structure in the interface GaAs-air are obtained according to the Eq. 4.1 and Eq. 4.2 and can be found in Table 7.3.

Grating Period (Λ)	23.3μm
Thickness (d)	33.32μm

Table 7.3: Size of the pyramids of the moth-eye structure

The resulting structure that has been simulated can be found in Fig.7.10, where only pyramids on the first Fresnel zone have been placed since, as it was said in Section 6.3, the best results were obtained for this position.

(a) Transversal cut

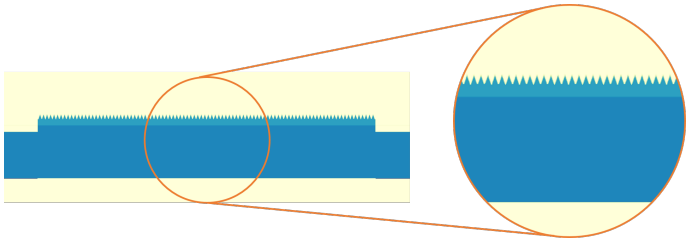

(b) Zoom centered in the moth-eye structure

Figure 7.10: Transversal views of the silicon FZP lens-antenna with a moth-eye structure

As it can be seen, in this case a base for the moth-eye structure had to be added at the top of the first Fresnel zone and underneath the pyramids in order to have the most realistic simulation, since the real glued silicon pyramids would need a base. This base has been chosen to have a thickness of $\lambda/2$, getting the 2D simulation results in Fig.7.11.
A better performance has been obtained again when using the moth-eye structure, achieving better coupling between the substrate and the air, a more directive beam and a cleaner field diagram. However, this design has not been considered for the first implementation due the complexity in fabrication of the moth-eye structure. Even though the material that has been chosen for the moth-eye structure, i.e. silicon, is one of the easiest to etch, the size of the pyramids, in the order of microns, and their triangular shape, do not make an easy implementation.

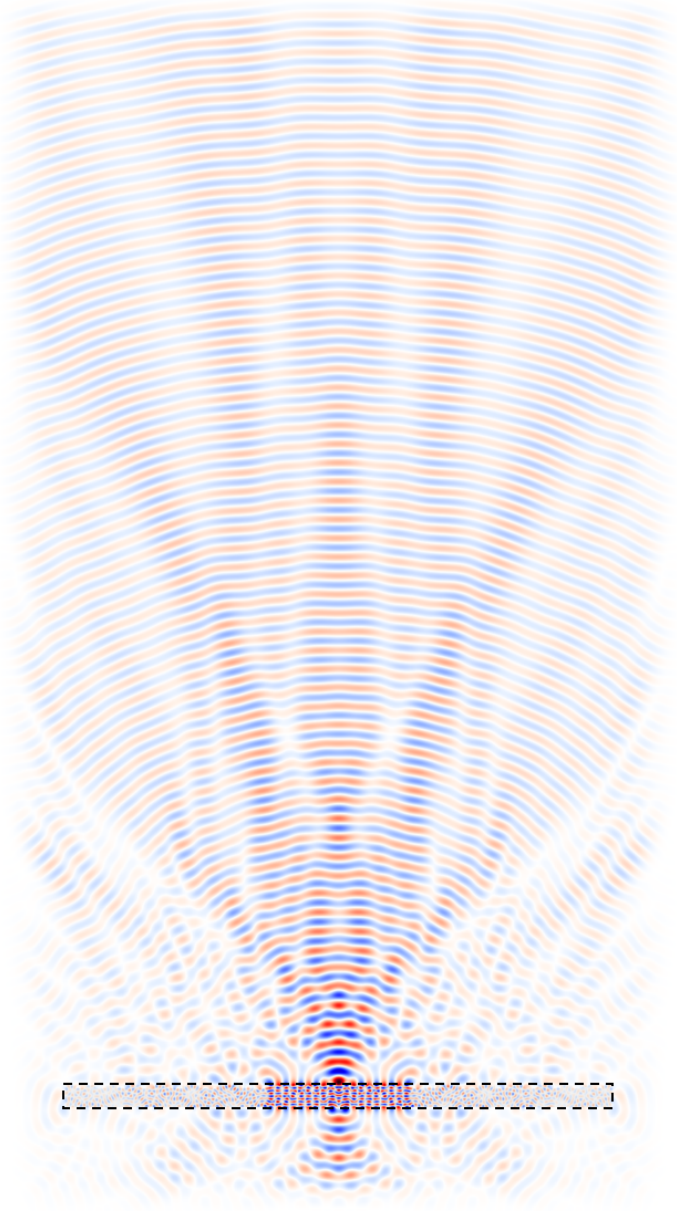

Figure 7.11: Electrical field distribution of the integrated FZP lens-antenna in LTG-GaAs with gold and a moth-eye structure

8 Implementation Process and Results

Throughout this paper, a series of options for the THz antenna for a nanocontacts based photomixer have been designed and simulated. Among all of them, one has been chosen to be implemented due to the characteristics that it presented in the simulations (detailed in Section 7.2) and the fabrication simplicity: the integrated FZP lens-antenna in LTG-GaAs with gold. In this chapter, a part of the process of the implementation that needs to be followed in the clean room, will be detailed, showing that this device can be produced in two simple fabrication steps of normal optical lithography.
For the lithography process, the mask that has been attached in the Appendix B has been fabricated. A real picture of it is shown in Fig. 8.1, where it can be seen that there are different antenna designs. The circular shapes that do not have any antenna in the middle will correspond to the top FZP of the design, and therefore, the focusing element (the same FZP designed in Chapter 7). Regarding the circular shapes that have an antenna, they correspond to the gold rings that are placed underneath the FZP. The antennas employed, as well as the integrated photomixers are different: log-periodic tooth and spiral antennas and interdigitated designs with different distances between the fingers and not interdigitated designs. Moreover, some alignment marks are placed, delimiting a square around the FZPs with the purpose of being able to align the top and bottom sides of the sample by dicing it.

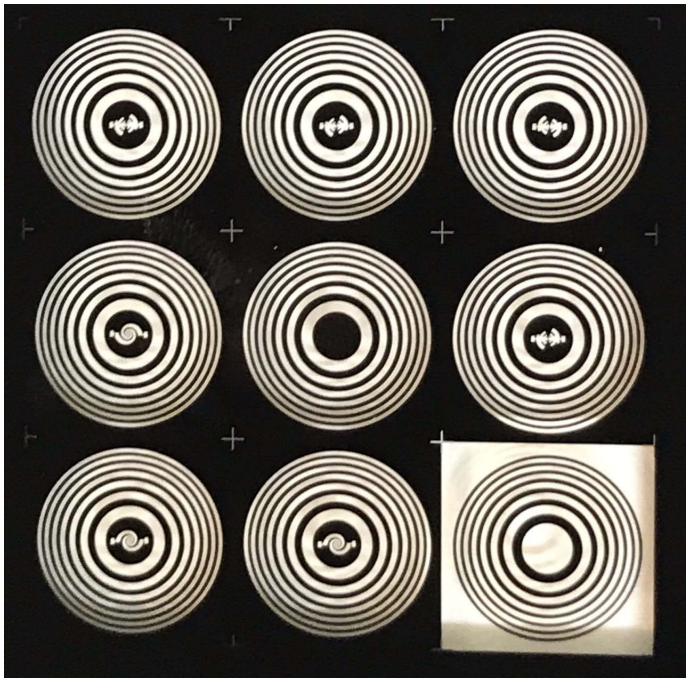

Figure 8.1: Top view of the fabricated mask

Therefore, the first step, after having cut and cleaned the GaAs, will consist on, by optical lithography, placing the FZP on the GaAs. For this purpose, the photoresist AZ 1518 has been used with 13 seconds of light exposure, and with around 18 seconds in the developer. After that, the etching must take place. A depth of 41.65μm is needed, according to what was calculated in Chapter 7, therefore, since it is a high amount, wet etching has been chosen as the best option. To do so, a solution of water, sulfuric acid and hydrogen peroxide, with the proportions of 100:10:80 ($H_2O : H_2SO_2 : H_2O_2$), respectively, is employed. The resulting etching depth after 10 minutes in the solution has been of 34μm, i.e. 3.4μm/min. This depth is not enough,

thus, more samples will have to be implemented to optimize the etching time to reach the desired etching depth. The results of this process are shown in Fig. 8.2, where the clean shape of the etched FZP is seen.

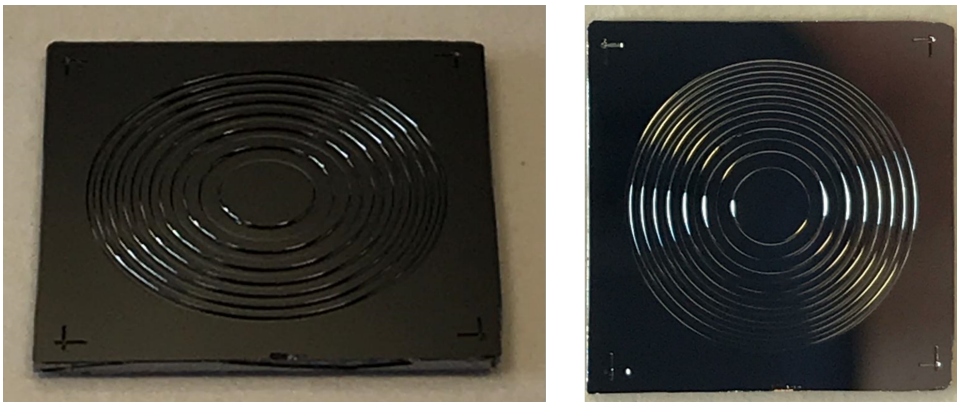

Figure 8.2: Top views of the etched FZP on GaAs

In Fig. 8.3 a zoom has been done in the center of the FZP, in order to appreciate better the circles that represent the Fresnel zones. It can be seen that almost perfect circles can be achieved by wet etching.

Figure 8.3: Zoomed etched FZP

The next step would be dicing the samples using the alignment marks mentioned before in order to align the top and bottom parts. On this bottom part, the gold rings and the integrated photomixer in the antenna will be placed, directly underneath the center of the first Fresnel zone (left picture of Fig. 8.3). The same lithography process from before must be followed in this case too. The last step would be to evaporate gold in order to cover the antenna and the rings. Unluckily, it was not possible to reach this point of the implementation process.
In order to be able to analyse the etched shape from the sides, some transversal cuts have been done. In Fig. 8.4, four of these cuts from the FZP can be seen: two centred in the first Fresnel zone, and two where more zones can be seen. The main point of this figure, is to appreciate that the etching does not generate perfectly perpendicular borders but with some inclination, making a difference with the simulations.
Other etching trials with different circular shapes have been done during this work, where this phenomena can be better appreciated. For this purpose, in Fig. 8.5, different cuts of a sample with an etched circle (Fig. 8.5a) have been done. Since the shape in this case is a circle, two sides of it will be underetched (Fig. 8.5b) but the two others will appear overetched on top (Fig. 8.5c).
Usually, this phenomenon deteriorates the behaviour of the implemented devices. In the case of the FZP, theoretically, it will benefit its behaviour due to the nature of the diffractive lenses, for which smoother changes in phase will generate a better focal point.

(a) Centered in the first Fresnel zone

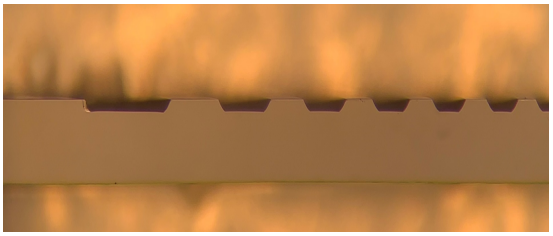

(b) Centered in outter rings

(c) Centered in the first Fresnel zone with a perspective

(d) Centered in outter rings with a perspective

Figure 8.4: Transversal cuts of the etched FZP

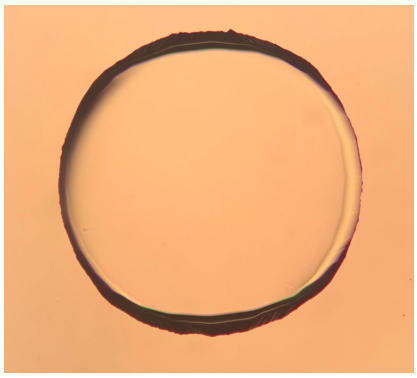

(a) Circle etched on GaAs

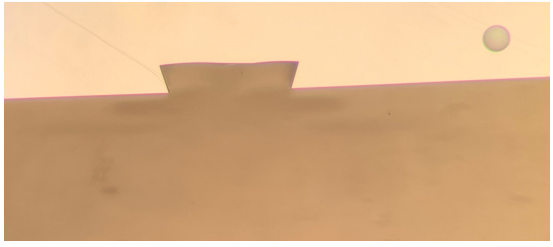

(b) Underetched border

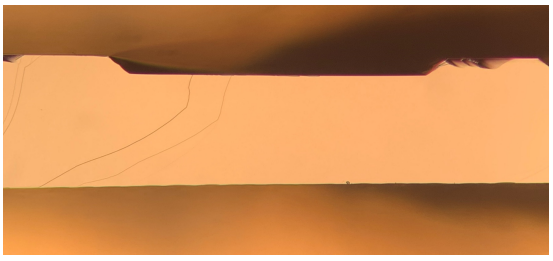

(c) Overetched border

Figure 8.5: Etched circle and its transversal cuts

9 Conclusions and Future Work

Applications in the THz range, like imaging, spectroscopy or future wireless communications demand more and more smaller systems in order to create compact and portable applications. This work was centred in the emitter part of a THz system, specifically in a nanocontacts based photomixer, which, as was detailed in Chapter 2, commonly uses a bulky silicon lens to create a directive THz wave.

One of the main aims here was to substitute this silicon lens by some planar type of lens. To do so, a FZP has been chosen among other considered options, like the photon sieves, due to its simplicity in fabrication and the possibilities in directivity that it offers. Moreover, a grooved kind of FZP has been employed so that more power would be collimated in the focal point. The results have been different devices that have been simulated with an FDTD software: Meep.

The designed devices have been split into two different groups: designs with a mounted lens (Chapter 6) and designs with an integrated lens (Chapter 7). In all of them, the main objective has been achieved, which was getting propagation and directivity, i.e. a focal point, with a smaller device.

Starting from the mounted lens-antenna designs, it was made clear in Section 6.2 that a FZP made out of silicon had a better performance than one made out of teflon (6.1) due to the fact that silicon has a higher refractive index and it is closer to the refractive index of LTG-GaAs. This also made possible having a smaller FZP in silicon than in teflon, which is convenient owing to the closeness of the source to the FZP. Furthermore, adding a moth-eye structure also made the performance of the mounted silicon lens-antenna device better.

However, since one of the main problems of using a common silicon lens is the misalignment between the source and the center of the lens, some other options were considered. The designs from Chapter 7 appear as a solution to the problem due to the integration of the FZP directly in the substrate that allows an implementation in only two simple fabrication technology processing steps (normal optical lithography). Moreover, the complete size of the device is reduced, from some centimetres with a common silicon lens to 8.8 mm of width with the FZP, and the bulkiness generated by the commonly used silicon lens is avoided.

The integrated FZP lens-antenna with gold (Section 7.2) gave a resulting directivity of 19.9 dBi at f=1067GHz in CST Studio, a bandwidth that goes from 300GHz to 3THz and a focal point that is not sensible to misalignments, which means directivity is accomplished, a bandwidth similar to the one of a common silicon lens is obtained and the focal point that was misplaced with a misalignment of the silicon lens is still centred. Thus, this device is presented as the best option for a first implementation.

The implementation process of the integrated FZP lens-antenna with gold that has to be followed is explained in Chapter 8, where first, an optical lithography step has to be done to etch the FZP, followed by a dicing of the sample to align top and bottom and concluding with a second optical lithography step for the photomixer and the bottom rings to evaporate gold on them. However, the gold evaporation and the measurements will remain as future work.

In the same line as the etched FZP and as future work, it could be interesting the usage of the photon sieves that are more complicated to design properly and also to implement. However, they present better directivity characteristics and reduce the propagation of higher orders of diffraction.

A Python Code

A.1 Code for the Integrated FZP Lens-Antenna in LTG-GaAs with Gold Simulations

```
#LIBRARIES
import meep as mp
import numpy as np
import matplotlib.pyplot as plt

import math


#VARIABLES

l0 = 0.3 #lamda

#Permitivitties
eps_base = 12.97
eps_FZP = eps_base

l = l0/math.sqrt(eps_base)
f = 15.0 #focal distance
w = 0.15 #resolution
n = (l*f)//(4*w*w) + 1

n = int(n)
print(n)

if n<5:
n = 8

if (n % 2) != 0:
n = n+3

else:
n = n+2


#Thicknesses
thickness_FZP = l/2
thickness_base = 0.35#0.35 - thickness_FZP
thickness_gold = 85e-6

##############       FUNCTIONS        ############


#Radius calculation of the rings
def radii_calc(n,l,f):
```

```
r = [0] * n
i = 0
while i < n:
a = i*l * (f + (i*l/4))
r[i] = math.sqrt(a)
i += 1

return r


##############       MAIN         ############


r = radii_calc(n,l,f)
print(r)

r_max = r[n-1]
print(r_max)


length_base = 2*r_max


geometry = [mp.Block(mp.Vector3(length_base,thickness_base,1e20),
center = mp.Vector3(0,0 +8.0),
material = mp.Medium(epsilon=eps_base))]


i = 0

while i < n-1:
if i == 0 or (i % 2) == 0:
geometry.append(mp.Block (mp.Vector3(2*r[n-i-1],thickness_FZP,1e20),
center = mp.Vector3(0,-thickness_base/2 + thickness_FZP/2 +8.0),
material = mp.Medium(epsilon = eps_FZP)
)
)

geometry.append(mp.Block (mp.Vector3(2*r[n-i-1],thickness_gold,1e20),
center = mp.Vector3(0,thickness_base/2 + thickness_gold/2 +8.0),
material = mp.air
)
)


else:
geometry.append(mp.Block (mp.Vector3(2*r[n-i-1],thickness_FZP,1e20),
center = mp.Vector3(0,-thickness_base/2 + thickness_FZP/2 +8.0),
material = mp.air
)
)

geometry.append(mp.Block (mp.Vector3(2*r[n-i-1],thickness_gold,1e20),
center = mp.Vector3(0,thickness_base/2 + thickness_gold/2 +8.0),
material = mp.Medium(D_conductivity = 3.5e-4, epsilon = 16000)
)
)
```

```
i += 1


sources = [mp.Source(mp.ContinuousSource(wavelength=l0, width=0.3),
component=mp.Ez,
center=mp.Vector3(0,thickness_base/2 +8.0),
size=mp.Vector3(0.3,0))]


pml_layers = [mp.PML(1.0)]
cell = mp.Vector3(2.5*r_max,20,0)
resolution = 180

sim = mp.Simulation(cell_size=cell,
boundary_layers=pml_layers,
geometry=geometry,
sources=sources,
resolution=resolution)


############# GENERATES ONLY THE EZ.h5 FILE #############
sim.use_output_directory()
sim.run(mp.at_beginning(mp.output_epsilon),
mp.to_appended("ez", mp.at_every(0.6, mp.output_efield_z)),
until=200)

#################### ONLY TO DRAW ######################

# sim.run(until=300)
#
# eps_data = sim.get_array(center=mp.Vector3(), size=cell, component=mp.Dielectric)
# plt.figure(dpi=100)
# plt.imshow(eps_data.transpose(), interpolation='spline36', cmap='binary')
# plt.axis()
# plt.show()
```

B Technical Drawings

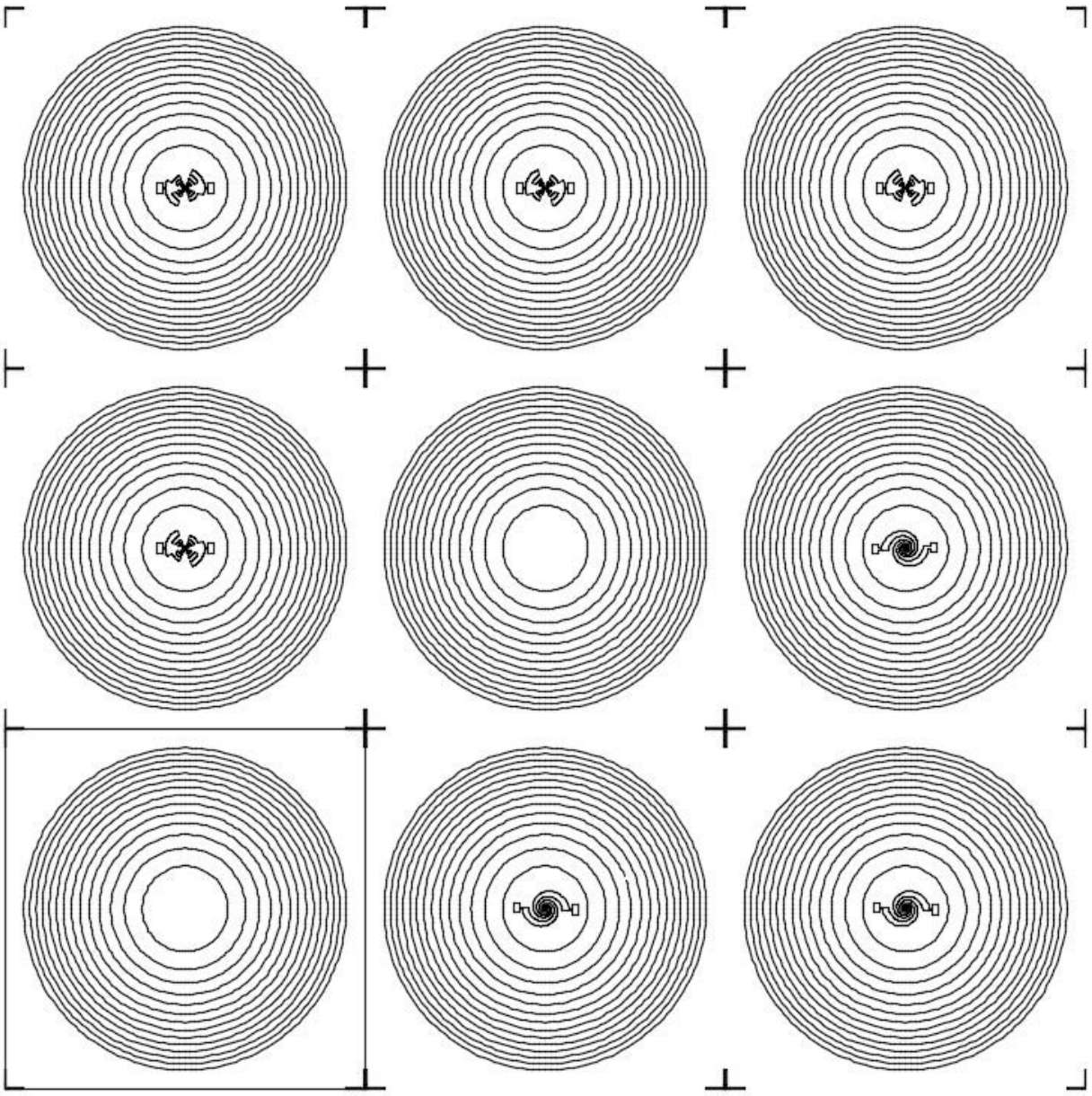

Figure B.1: Fabricated mask

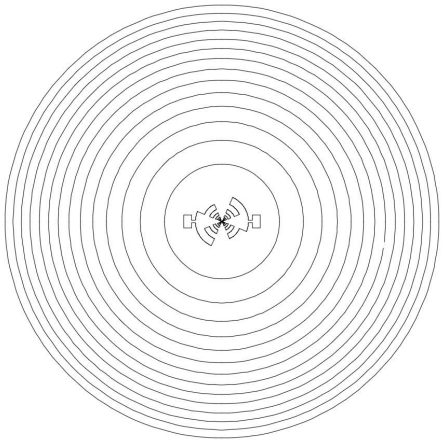

(a) Log-periodic tooth antenna photomixer with gold rings

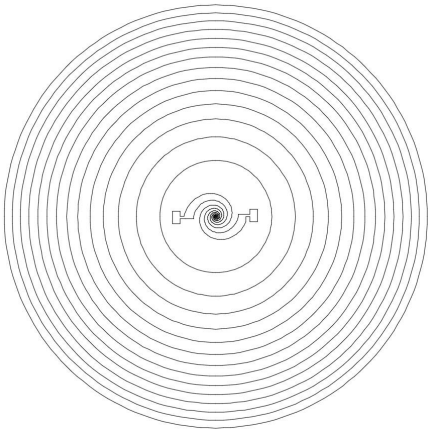

(b) Log-periodic spiral antenna photomixer with gold rings.

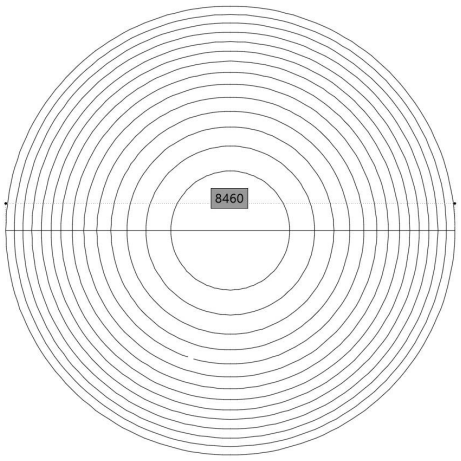

(c) FZP with size of the biggest zone (positive mask)

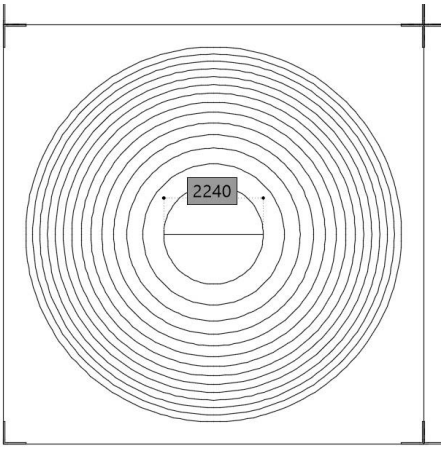

(d) FZP with size of the smallest zone (negative mask)

Figure B.2: Details of the fabricated mask

Bibliography

[1] J. Xu, Z. N. Chen, and X. Qing, "270-GHz LTCC-integrated high gain cavity-backed fresnel zone plate lens antenna," *IEEE Transactions on Antennas and Propagation*, vol. 61, no. 4, pp. 1679–1687, 2013.

[2] S. Al-Daffaie, O. Yilmazoglu, F. Küppers, and H. L. Hartnagel, "1-D and 2-D nanocontacts for reliable and efficient terahertz photomixers," *IEEE Transactions on Terahertz Science and Technology*, vol. 5, no. 3, pp. 398–405, 2015.

[3] C. Yu, S. Fan, Y. Sun, and E. Pickwell-MacPherson, "The potential of terahertz imaging for cancer diagnosis: A review of investigations to date," *Quantitative Imaging in Medicine and Surgery*, vol. 2, no. 1, pp. 33–45, 2012. [Online]. Available: http://qims.amegroups.com/article/view/106/116

[4] S. Al-Daffaie and Internationaler Fachverlag für Wissenschaft & Praxis., *Nanoelectrode Based Photomixer for Continuous Wave Terahertz Generation*.

[5] C. Sydlo, *Reliability investigations and development of compound semiconductor devices for microwave and terahertz applications*. Shaker, 2006.

[6] C. A. Balanis, *Antenna Theory. Analysis and Design*, fourth edi ed., Hoboken, New Jersey, 2016.

[7] O. V. M. Igor V. Minin, *Basic Principles of Fresnel Antenna Arrays*, ser. Lecture Notes Electrical Engineering. Berlin, Heidelberg: Springer Berlin Heidelberg, 2008, vol. 19.

[8] T. Yellman, "On Frequency," *Risk Analysis*, vol. 32, no. 3, pp. 363–367, 2012.

[9] D. This, "Design and analysis of integrated lens antennas FACULTY OF ELECTRICAL ENGINEERING TELECOMMUNICATIONS DIVISION EC Design and analysis of integrated lens antennas," 1997.

[10] "Fresnel zone plate theory." [Online]. Available: http://zoneplate.lbl.gov/theory

[11] C. Between, D. Power, D. Designs, O. Works, O. High, D. Ratio, A. Minakawa, M. Muraguchi, T. Symposium, A. Technol, and S. Clara, "Antennas Loaded With a Coupling Strip and Lumped Elements for," *Microwave and Optical Technology Letters*, vol. 55, no. 2, pp. 363–366, 2013.

[12] R. Adelung, L. Kipp, R. L. Johnson, M. Skibowski, S. Harm, R. Seemann, and R. Berndt, "Sharper images by focusing soft X-rays with photon sieves," *Nature*, vol. 414, no. 6860, pp. 184–188, 2002.

[13] "Photon Sieves - New Way of focusing FEL Radiation." [Online]. Available: http://photon-science.desy.de/research/research{_}highlights/archive/photon{_}sieves/index{_}eng.html

[14] "MPSS | EL Seed." [Online]. Available: http://elseed.com/products/mpss/

[15] "Moth Eyes Inspire Improvements in Thin Films | Architect Magazine | Research." [Online]. Available: https://www.architectmagazine.com/technology/moth-eyes-inspire-improvements-in-thin-films{_}o

[16] R. Brunner, O. Sandfuchs, C. Pacholski, C. Morhard, and J. Spatz, "Lessons from nature: Biomimetic subwavelength structures for high-performance optics," *Laser and Photonics Reviews*, vol. 6, no. 5, pp. 641–659, 2012.

[17] C. Brückner, B. Pradarutti, S. Riehemann, O. Stenzel, R. Steinkopf, A. Gebhardt, G. Notni, and A. Tünnermann, "Moth-eye structures for reduction of Fresnel losses at THz components," vol. 6194, pp. 1–11, 2006.

[18] T. A. Milligan, *Modern Antenna Design*, 2005.

[19] C. Warren, S. Sesnic, A. Ventura, L. Pajewski, D. Poljak, and A. Giannopoulos, "Comparison of Time-Domain Finite-Difference, Finite-Integration, and Integral-Equation Methods for Dipole Radiation in Half-Space Environments," *Progress In Electromagnetics Research M*, vol. 57, no. February, pp. 175–183, 2017.

[20] N. Laman and D. Grischkowsky, "Terahertz conductivity of thin metal films," *Applied Physics Letters*, vol. 93, no. 5, pp. 1–4, 2008.

List of Figures

List of Tables